Transmission Radius Control in Wireless Ad Hoc Networks with Smart Antennas

Fei Huang, *Student Member, IEEE,* Ka-Cheong Leung, *Member, IEEE,* and Victor O. K. Li, *Fellow, IEEE*

***Abstract*—In this paper, we present a model to analyze the performance of three transmission strategies with smart antennas, i.e. directional antennas with adjustable transmission power. Generally, a larger transmission radius contributes a greater progress if a transmission is successful. However, it has a higher probability of collision with other concurrent transmissions. Smart antennas mitigate collisions with sectorized transmission ranges. They also extend the transmission radii. By modelling three transmission strategies, namely, Nearest with Forward Progress (NFP), Most Forward with Fixed Radius (MFR), and Most Forward with Variable Radius (MVR), our analysis illustrates that the use of smart antennas can greatly reduce the possibility of conflicts. The model considers the interference range and computes the interference probability for each transmission strategy. We have analyzed two Medium Access Control (MAC) protocols using our interference model, namely, the slotted ALOHA protocol and the slotted CSMA/CA-like protocol. The result shows that, for slotted ALOHA, NFP yields the best one-hop throughput, whereas MVR provides the best average forward progress. The overall performance is substantially improved with the slotted CSMA/CA-like protocol, and the network becomes more resilient.**

***Index Terms*—Ad hoc networks, interference ratio, smart antenna.**

I. Introduction

In a wireless ad hoc network, a group of communication nodes are allowed to set up and maintain in the network among themselves, without the support of a base station or a central controller [8].

One of the challenges in wireless ad hoc network is limited power supply (e.g. battery). Therefore, optimizing the transmission radius with power control can achieve the most economical use of energy [23]. It can also improve network performance by reducing the interference. Two transmission strategies, namely, Nearest with Forward Progress (NFP) and Most Forward with Variable Radius (MVR), use adjustable transmission power. The key measurement of the performance of these two strategies is forward progress, and one aims to identify the optimal per-hop transmission range to yield the maximal energy efficiency [4], [6]. The transmission range control analysis for NFP, MVR, and another strategy named Most Forward with Fixed Radius (MFR) with omni-directional antennas has been investigated in [6]. Adopting slotted ALOHA as the Medium Access Control (MAC) protocol, [6] showed that NFP yields the best throughput in a high terminal density environment. The strategy is best suited for applications in road traffic information systems, such as cooperative driving by data exchange between neighbouring vehicles. These applications generally demand high network bandwidth for real time reliable data exchange [16].

Besides energy conservation with power control, smart antennas can improve the network throughput by spatial reuse [18], [22]. In [13], the network throughput is surprisingly low when omni-directional antennas are used at each node. It has been shown [18] that the adoption of smart antennas in wireless ad hoc networks can significantly improve the network performance, since it greatly reduces the radio interference. There are two different modes of operation for a node installed with a smart antenna. They are the omni-directional mode (OMNI-mode) and beam-forming mode (BF-mode). In OMNI-mode, the antenna sends and receives signals over all directions. In BF-mode, the antenna sends and receives signals through a beam pattern. The interference is mainly determined by the main lobe (and perhaps some of the side lobes) of the beam. In our work, the term “smart antenna" refers to the Adaptive Antenna Array (AAA) with steerable beam and adjustable transmission power. The antenna weights of AAA can be dynamically adjusted so that the beam pattern is optimized for the reception of the desired signal and nulling of interference [3].

An analytical model extended from [6] for directional antennas has been devised in [24], but it only considers the MFR strategy. The results in [24] have shown that directional antennas perform better than omni-directional antennas in a high node density environment. In [6], [24], the transmission range (or area of coverage) is assumed to be equal to the interference range. However, in practice, some nodes may still interfere with the receiver even when the receiver is outside the transmission ranges of these nodes [20]. In our work, we relax this assumption so that the interference range can be larger than the transmission range and focus on the transmission radius control analysis in wireless ad hoc networks using smart antennas.

In our previous paper [7], we proposed an analytical model for wireless ad hoc networks with smart antennas and analyze the performance of NFP. In this paper, we extend our analytical model to three transmission strategies, namely, NFP, MVR, and MFR. Our results show that NFP yields the highest one-hop throughput, whereas MVR provides the largest average forward progress.

The rest of the paper is organized as follows. In Section II,

Paper approved by K. Leung, the editor for Wireless Network Access and Performance of the IEEE Communications Society. Manuscript received November 20, 2008; revised August 20, 2009 and December 18, 2009.

This research is supported in part by the Research Grants Council of the Hong Kong Special Administrative Region, China, under Grant No. 7152/05E.

The authors are with the Department of Electrical and Electronic Engineering, The University of Hong Kong, Pokfulam Road, Hong Kong, China (e-mail: feihuang@eee.hku.hk, kcleung@ieee.org, vli@eee.hku.hk).

Digital Object Identifier 10.1109/TCOMM.2010.062510.080600

we introduce the network model for our analysis. In Section III, the probability of interference is computed for each transmission strategy. The performance analysis is presented in Section IV. Finally, we conclude in Section V.

II. Network Model

Our analytical model is based on the premise that each node knows the locations of all other nodes in the network. The simplest way for a node to find its exact location is to use Global Positioning System (GPS) [10]. This information can then be sent to other nodes, for example, by being piggybacked on outgoing packets. A sender will pick one of its neighbours as a relay according to one of the three strategies and transmit a packet with the identity (ID) of the relay and the ID of the final destination in the packet header. A sectorized beam pattern is formed by the sender toward the intended receiver. In each time slot, a node with no packet to send listens to the channel omni-directionally and receives the packet omni-directionally if chosen as a receiver [19]. A neighbouring node receiving this packet will process the packet only if it is identified as a relay or a final destination. All other neighbours will discard the packet. A separate channel is available for acknowledgement. Furthermore, whenever there is a packet waiting to be sent, it is equally likely that this packet will be destined to any other node. Relevant terminologies are defined as follows.

A. Antenna Model and Maximum Transmission Radius R

A smart antenna consists of a main lobe and several parasitic side lobes which may cause harmful interference to other receivers in its vicinity. However, the side lobes can be steered toward areas without nodes owing to the adaptability of the directional antenna beams [12]. For simplicity, side lobes are neglected in the rest of the paper. Without the side lobes, existing work, such as [25], generally models the beam pattern of a smart antenna as a semi-elliptic region. In this paper, the beam pattern is modelled as a sector for the simplicity of the analysis [4].

By using smart antennas, the transmission radius is extended by shaping the transmission range into a sector. Given the same amount of power, smart antennas can transmit farther than the omni-directional ones. Let R and R_{omni} be the maximum transmission radii of a smart antenna and an omni-directional antenna, respectively. We assume that the transmission ranges or regions covered by smart and omni-directional antennas are approximately the same. Therefore,

$$R \approx \sqrt{\frac{2\pi (R_{\text{omni}})^2}{\beta}} \tag{1}$$

where β is the beam-width of a smart antenna such that $\beta \in (0, 2\pi]$.

B. Transmission Direction and Range

Node A with a smart antenna can transmit in a range shaped as a sector with an angle β. This is called the transmission range of A. The centreline of the sector is defined as the transmission direction of Node A. The transmission radius falls between 0 and R.

C. Interference Range to Transmission Range Ratio

Generally speaking, the interference range of a node is not necessarily equal to the transmission range. When Node A is transmitting with an angle of β and a radius of R_x, the interference range of A is a sector with an angle of α and a radius of R_I, where $R_I \geq R_x$ and $\alpha \geq \beta$. The transmission direction of A is also the centreline of its interference range. Any node in the transmission range of A can receive A's signal. However, a node in the interference range but outside the transmission range of A cannot receive A's signal successfully but it will be interfered by the signal. Any node outside the interference range of A will not be affected by the transmission of A. Furthermore, we assume that all interferences to a receiving node from different directions are equal if they have the same transmission distances. In reality, there is no practical smart antenna which can provide equal gain for all directions [21]. For mathematical tractability, we assume that an ideal antenna beam has a constant gain in all directions within its transmission range.

We set two parameters, namely, a_R and a_β, to define the interference range of a node. Specifically, $a_R = \frac{R_I}{R_x}$ and $a_\beta = \frac{\alpha}{\beta}$. Here,

$$\alpha = \begin{cases} a_\beta \beta, & a_\beta \beta \in (0, 2\pi] \\ 2\pi, & a_\beta \beta \in (2\pi, \infty) \end{cases} \tag{2}$$

If $R_x = R$, R_I equals $a_R R$, which is the maximum interference radius of a node. We define the circle centred at A with a radius of $a_R R$ as the maximum interference range of A. Any nodes within this range may potentially be interfered by the transmission of A. Furthermore, we define these nodes as the neighbours of A. It is possible that several non-neighbouring nodes transmit in the same slot and their add-up interference exceeds the threshold of interference. But to simplify the analysis, we do not consider the interference effects from non-neighbouring nodes.

This paper is an extension of the work in [6], with the consideration of the characteristics of smart antennas. Some studies, such as [18], account for the fading and shadowing effects when formulating the interference model in the analysis wherein the signal to interference and noise ratio (SINR) at a certain point around the receiving node is time-varying. However, in order to simplify the model and make the analysis mathematically tractable, we have assumed that a_R and a_β are constants. In other words, SINR will not change with time.

D. Forward Progress

The forward progress of a transmitter A to a receiver B is defined as the distance between A and B projected onto a line drawn from A towards its final destination C [6]. As exhibited in Fig. 1, the forward progress of A to B is Z.

As shown in Fig. 1, Line AC is defined as the forward direction of A, where C is the final destination of Node A. The middle line is perpendicular to the Line AC, and cuts the maximum interference range of A into two halves. The shaded semicircle is called the forward semicircle of A, and the other one is called the backward semicircle of A. Any receiver in the intersection of the forward semicircle and the

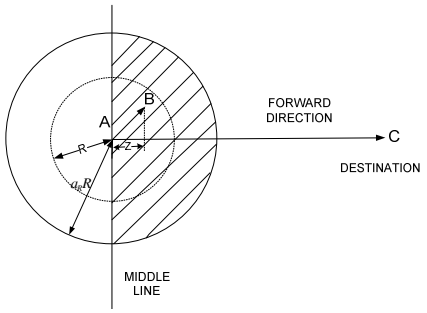

Fig. 1. An illustration for the forward progress, semicircle, and middle line.

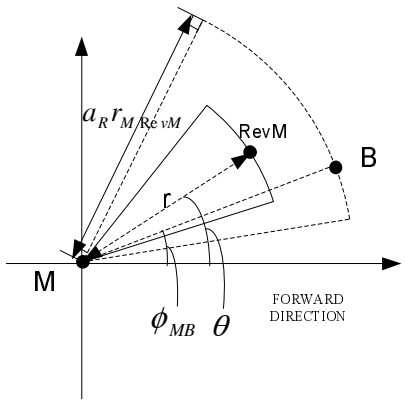

Fig. 2. An illustration of *B* being interfered by *M*.

maximum transmission range of A can provide nonnegative forward progress to A. Note that the forward semicircle is a portion of the maximum interference range, while the receivers of Node A can only exist within the maximum transmission range of A.

Node A will transmit only if it can find an eligible receiver in its forward semicircle as shown in Fig. 1, since any receiver in A's backward semicircle cannot contribute a positive forward progress.

E. Node Distribution

All nodes in the network are distributed as a two-dimensional Poisson point process with density λ (nodes per unit area).

- Define N, the mean number of nodes within an area of πR^2, as the network connectivity. Thus, λ equals $\frac{N}{\pi R^2}$.
- The probability of finding i nodes in an area of size G is $\frac{(\lambda G)^i \cdot e^{-\lambda G}}{i!}$, where i = 1, 2, 3, ...
- Let $A+$ be the event that Node A can find an eligible receiver in the forward semicircle. By [6], $P_r(A+) = 1 - \frac{(\lambda \frac{1}{2}\pi R^2)^0 \cdot e^{-\lambda \frac{1}{2}\pi R^2}}{0!} = 1 - e^{-\frac{N}{2}}$.

F. MAC Protocols

We are going to analyze two MAC protocols using our interference model. The first one is slotted ALOHA, which is often used in subscriber-based satellite communication networks and contactless RFID technologies [15]. We assume that all nodes always have packets to send. Time is divided into slots. In every time slot, each node tries to transmit according to the Bernoulli process with parameter p, where $0 < p \leq 1$.

The second one is the slotted CSMA/CA-like protocol. It is a simplified version of the slotted Carrier Sense Multiple Access with Collision Avoidance (CSMA/CA) protocol adopted in IEEE 802.15.4, which is widely used in low-rate wireless personal area networks [1], [6]. Each node in the network generates packets from its upper layer according to the Bernoulli process with parameter p, where $0 < p \leq 1$. At the beginning of each slot, two mini-slots, namely, m-slot1 and m-slot2, are allocated for nodes to transmit Request to Send (RTS) and Clear to Send (CTS) packets. The remaining duration of a time slot is used for data communication. Nodes will transmit an RTS packet in m-slot1 with probability p. The RTS packet is sent in BF-mode pointing to the intended receiver. If the receiver is available to receive a data packet, it will respond to the sender by replying with a directional CTS packet. If no CTS packet is received by the end of m-slot2, the sender will refrain from transmitting data for the current time slot.

III. Probability of Interference

A. Analysis of Interference

Suppose Node A wants to send a packet to its final destination C, and B is the first relay of this packet. Thus, a transmission occurs from Node A to Node B. For this transmission to be successful, B cannot be covered by the interference range of any other transmitting node.

Let M be one of B's neighbours other than A and also M has a packet to be sent. By the network model described in Section II, we know that neighbours of a node are uniformly distributed in the maximum interference range of that node. However, given a transmission from A to B, there is an area where no nodes exist. This area is a function of B with respect to A, and is called the excluded region (see Section IV). Since no node can be in the excluded region, B is not uniformly distributed within the maximum interference range of M. To simplify the analysis, we make the approximation that B is uniformly distributed within the maximum interference range of M. As we can see in Section IV, this approximation is reasonable since the discrepancy between the analytical and simulation results is pretty small ($< 5\%$). Define a polar coordinate system with respect to M. Denote the polar coordinates of B as $B(r_{MB}, \phi_{MB})$, where r_{MB} is the distance between M and B, and ϕ_{MB} is the polar angle measured from the forward direction of M (which is the direction to the final destination of the packet sent by M) to the direction to reach B, as shown in Fig. 2.

By [6], the probability density functions of r_{MB} and ϕ_{MB} are computed as:

$$f_{r_{MB}}(r_{mb}) = \frac{2\pi r_{mb}}{\pi(a_R R)^2} = \frac{2r_{mb}}{(a_R R)^2}, \quad r_{mb} \in (0, a_R R] \tag{3}$$

$$f_{\phi_{MB}|r_{MB}}(\phi_{mb}|r_{mb}) = \frac{1}{2\pi}, \quad \phi_{mb} \in [0, 2\pi) \tag{4}$$

Thus,

$$\begin{aligned} f_{r_{MB},\phi_{MB}}(r_{mb}, \phi_{mb}) &= f_{r_{MB}}(r_{mb}) \cdot f_{\phi_{MB}|r_{MB}}(\phi_{mb}|r_{mb}) \\ &= \frac{r_{mb}}{\pi(a_R R)^2} \end{aligned} \tag{5}$$

B. Probability of Interference for NFP

In NFP, the transmitter chooses the nearest node that can provide positive forward progress as the intended receiver. The transmission radius is just the distance between the transmitter and the intended receiver. With a smaller transmission radius, the interference range is substantially reduced. Let I be the event that B gets interfered by M.

The maximum interference range of M is divided into four divisions. Let r_i be the distance between Node M and an arbitrary node B in Division i, where i = 1, 2, 3, 4. Let θ_i be the polar angle measured from the forward direction of M to the line segment *MB*. We define the four divisions as:

Division 1: $r_i \in (R, a_R R], \theta_i \in [-\frac{\pi}{2}, \frac{\pi}{2}]$

Division 2: $r_i \in (R, a_R R], \theta_i \in (\frac{\pi}{2}, \pi] \cup (-\pi, -\frac{\pi}{2})$

Division 3: $r_i \in (0,\ R], \theta_i \in [-\frac{\pi}{2}, \frac{\pi}{2}]$

Division 4: $r_i \in (0, R], \theta_i \in (\frac{\pi}{2}, \pi] \cup (-\pi, -\frac{\pi}{2})$

The probability of I is computed based on these four divisions. That is, the probability of I is the sum of four probabilities, each of which corresponds to the case that B is in one of the four divisions and gets interfered. Let $Div(i)$ be the event that B is in Division i, where i = 1, 2, 3, 4. According to the Law of Total Probability, we can get:

$$P_r(I) = \sum_{i=1}^{4} P_r(I, Div(i)) \tag{6}$$

1) Computation of $P_r(I, Div(1))$: In this case, $P_r(I, Div(1))$ is the probability that B is in Division 1 and gets interfered by M.

Let $RevM$ be the receiver of M. Here, $RevM$ is the first relay of the packet sent by M. r_M is the transmission radius of M. By [6], the probability density function of a receiver's position for a transmission using NFP can be computed as:

$$f_{r,\theta}^{NFP}(r_0, \theta_0) = \frac{\lambda r_0 e^{-\frac{\lambda \pi r_0^2}{2}}}{1 - e^{-\frac{N}{2}}}, r_0 \in (0, R], \theta_0 \in [-\frac{\pi}{2}, \frac{\pi}{2}] \tag{7}$$

where r and θ are the distance between M and $RevM$, and the transmission angle of M, respectively. The transmission angle of a node is defined as the polar angle measured from the forward direction to its transmission direction. Note that the transmission radius r_M is equal to r in NFP. That is, r_M = r.

The probability of the event $\{I, Div(1)\}$ is equivalent to the probability of the event $\{M+, B \in \Psi_{M \to RevM}, Div(1)\}$, where $M+$ is the event that M can find an eligible receiver, and $B \in \Psi_{M \to RevM}$ is the event that Node B is in the interference range of the transmission from M to $RevM$. $P_r(M+)$ is the probability that Node M can find an eligible receiver in the forward semicircle. Now, $P_r(M+) = 1 - e^{-\frac{N}{2}}$. The event $\{B \in \Psi_{M \to RevM}, Div(1)|M+\}$ occurs when the following three conditions are all satisfied:

- $r_{MB} \in (R, a_R R]$ and $\phi_{MB} \in [-\frac{\pi}{2}, \frac{\pi}{2}]$
- $r < r_{MB} < a_R \cdot r_M$
- $|\theta - \phi_{MB}| \le \frac{\alpha}{2}$

The first condition is for Node B to be in Division 1. Conditions 2 and 3 specify B to be in the interference range of the transmission from M to *RevM*, i.e. $B \in \Psi_{M \to RevM}$.

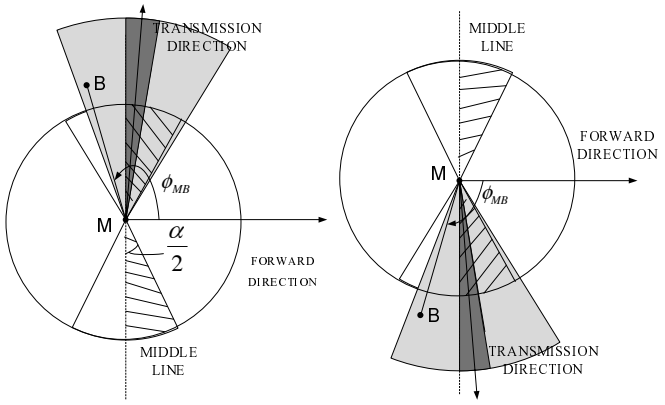

(a) $\phi_{MB} \in (\frac{\pi}{2}, \frac{\pi}{2} + \frac{\alpha}{2}]$. (b) $\phi_{MB} \in (-\frac{\pi}{2} - \frac{\alpha}{2}, -\frac{\pi}{2}]$.

Fig. 3. An illustration for B in the backward semicircle of M.

Since r is the distance between M and *RevM*, $r \in (0, R]$. As $r_M = r$ and $r < r_{MB} \le a_R r_M$, we can get $\frac{r_{MB}}{a_R} \le r \le R$. Therefore,

$$\begin{aligned}
&P_r(I, Div(1)) \\
=&P_r(M+, B \in \Psi_{M \to RevM}, Div(1)) \\
=&P_r(M+) \cdot P_r(B \in \Psi_{M \to RevM}, Div(1)|M+) \\
=&P_r(M+) \cdot P_r(B \in \Psi_{M \to RevM}|Div(1), M+) \\
&\cdot P_r(Div(1)|M+) \\
=&P_r(M+) \cdot \int_R^{a_R R} \int_{-\frac{\pi}{2}}^{\frac{\pi}{2}} f_{r_{MB}, \phi_{MB}}(r_{mb}, \phi_{mb}) \\
&\cdot P_r(B \in \Psi_{M \to RevM}|Div(1), M+) d\phi_{mb} dr_{mb} \\
=&(1 - e^{-\frac{N}{2}}) \cdot \int_R^{a_R R} \int_{-\frac{\pi}{2}}^{\frac{\pi}{2}} \frac{r_{mb}}{\pi (a_R R)^2} \\
&\cdot \int_{\frac{r_{mb}}{a_R}}^{R} \int_{\phi_1}^{\phi_2} f_{r,\theta}^{NFP}(r_0, \theta_0) d\theta_0 dr_0 d\phi_{mb} dr_{mb} \\
=&\frac{\lambda}{\pi (a_R R)^2} \cdot \int_R^{a_R R} \int_{-\frac{\pi}{2}}^{\frac{\pi}{2}} \int_{\frac{r_{mb}}{a_R}}^{R} \int_{\phi_1}^{\phi_2} r_{mb} \cdot r_0 \\
&\cdot e^{-\frac{\lambda \pi r_0^2}{2}} d\theta_0 dr_0 d\phi_{mb} dr_{mb}
\end{aligned} \tag{8}$$

where $\phi_1 = max\{(\phi_{mb} - \frac{\alpha}{2}), -\frac{\pi}{2}\}$ and $\phi_2 = min\{(\phi_{mb} + \frac{\alpha}{2}), \frac{\pi}{2}\}$.

Since M will only transmit in its forward semicircle, there are boundary effects when B is located close to the middle line of M. For example, when $\phi_{MB} = \frac{\pi}{2}$, the range of integration on θ should be $[\frac{\pi}{2} - \frac{\alpha}{2}, \frac{\pi}{2}]$. Since the probability density function $f_{r,\theta}^{NFP}(r_0, \theta_0)$ will be non-zero only for θ in the range of $[-\frac{\pi}{2}, \frac{\pi}{2}]$, we have $\phi_1 = max\{(\phi_{mb} - \frac{\alpha}{2}), -\frac{\pi}{2}\}$ and $\phi_2 = min\{(\phi_{mb} + \frac{\alpha}{2}), \frac{\pi}{2}\}$.

2) Computation of $P_r(I, Div(2))$: In this case, $P_r(I, Div(2))$ is the probability that B is in Division 2 and gets interfered by M.

B will be interfered only if the interference range of M is extended to the backward semicircle as exhibited in Fig. 3. We can see that when the transmission direction of M is within either of the dashed areas, each of which is a sector with an angle of $\frac{\alpha}{2}$, its interference range will spread to the backward semicircle. In the extreme case, when the transmission direction of M is on its middle line, half of its interference range, which is a sector with an angle of $\frac{\alpha}{2}$, will be in the backward

semicircle. The event $\{B \in \Psi_{M \to RevM}, Div(2)|M+\}$ occurs when the following three conditions are all satisfied:

- $r_{MB} \in (R, a_R R]$ and $\phi_{MB} \in [\frac{\pi}{2}, \frac{\pi}{2} + \frac{\alpha}{2}] \cup \phi_{MB} \in (-\frac{\pi}{2} - \frac{\alpha}{2}, -\frac{\pi}{2}]$
- $0 < r_{MB} < a_R \cdot r_M$
- $|\theta - \phi_{MB}| \leq \frac{\alpha}{2}$

Since $r \in (0, R]$, $r_M = r$, and $r < r_{MB} \leq a_R r_M$, we can get $\frac{r_{MB}}{a_R} \leq r < R$.

There are two different cases on α (where α is the interference angle), namely, $\alpha \in (0, \pi]$ and $\alpha \in (\pi, 2\pi]$. Consider the case when $\alpha \in (0, \pi]$. For $\phi_{MB} \in (\frac{\pi}{2}, \frac{\pi}{2} + \frac{\alpha}{2}]$, an edge of the interference range of *M* being within $[\phi_{MB}, \frac{\pi}{2} + \frac{\alpha}{2}]$ will make the interference range of *M* cover *MB* as shown in Fig. 3(a), where the interference range of *M* is the shaded sector. It corresponds to the case that *M*'s transmission direction is within the range $[\phi_{MB} - \frac{\alpha}{2}, \frac{\pi}{2}]$ as shown in the dark grey sector in Fig. 3(a). For $\phi_{MB} \in (-\frac{\pi}{2} - \frac{\alpha}{2}, -\frac{\pi}{2}]$, an edge of the interference range of M being within $[-\frac{\pi}{2} - \frac{\alpha}{2}, \phi_{MB}]$ will make the interference range of M cover *MB* as shown in Fig. 3(b). It corresponds to the case that M's transmission direction is within the range $[-\frac{\pi}{2}, \phi_{MB} + \frac{\alpha}{2}]$ as shown in the dark grey sector in Fig. 3(b).

Thus, when $\alpha \in (0, \pi]$, $P_r(I, Div(2))$ can be computed as (9), shown in the next page.

When $\alpha \in (\pi, 2\pi]$, the edge of the interference range of M being within either $[\phi_{MB}, \frac{\pi}{2} + \frac{\alpha}{2}]$ or $[-\frac{\pi}{2} - \frac{\alpha}{2}, \phi_{MB}]$ can possibly make the interference range of M cover *MB*. It corresponds to the case that M's transmission direction is within the range $[\phi_{MB} - \frac{\alpha}{2}, \frac{\pi}{2}] \cup [-\frac{\pi}{2}, \phi_{MB} + \frac{\alpha}{2}]$.

When $\phi_{MB} \in [\frac{\pi}{2}, \frac{\pi}{2} + \frac{\alpha}{2}] \cup (-\frac{\pi}{2} - \frac{\alpha}{2}, -\frac{\pi}{2}]$ and $r_{MB} \in (R, a_R R]$, we can get (10) and (11), shown in the next page.

3) Computation of $P_r(I, Div(3))$: In this case, $P_r(I, Div(3))$ is the probability that B is in Division 3 and gets interfered by M.

Since B is within the intersection of the maximum transmission range and forward semicircle of M, M can always find a receiver to which a packet is sent. The probability of the event $\{I, Div(3)\}$ is equivalent to the probability of the event $\{B \in \Psi_{M \to RevM}, Div(3)\}$.

In Fig. 4, the largest sector is the interference range of M. Since $RevM$ is the closest node to M in NFP, r must be less than r_{MB}. The event $\{B \in \Psi_{M \to RevM}, Div(3)\}$ occurs when the following three conditions are all satisfied:

- $r_{MB} \in (0, R]$ and $\phi_{MB} \in [-\frac{\pi}{2}, \frac{\pi}{2}]$
- $r < r_{MB} < a_R \cdot r_M$
- $|\theta - \phi_{MB}| \leq \frac{\alpha}{2}$

Since $r \in (0, R]$, $r_M = r$, and $r < r_{MB} \leq a_R r_M$, we can get $\frac{r_{MB}}{a_R} \leq r < r_{MB}$.

$P_r(I, Div(3))$ can be determined as (12), shown in the next page, where $\phi_1 = max\{(\phi_{mb} - \frac{\alpha}{2}), -\frac{\pi}{2}\}$ and $\phi_2 = min\{(\phi_{mb} + \frac{\alpha}{2}), \frac{\pi}{2}\}$. Note that the boundary effect of θ is the same as that in Section III-B.1.

4) Computation of $P_r(I, Div(4))$: In this case, $P_r(I, Div(4))$ is the probability that B is in Division 4 and gets interfered by M.

The event $\{B \in \Psi_{M \to RevM}, Div(4)|M+\}$ occurs when the following three conditions are all satisfied:

- $r_{MB} \in (0, R]$ and $\phi_{MB} \in [\frac{\pi}{2}, \frac{\pi}{2} + \frac{\alpha}{2}] \cup \phi_{MB} \in (-\frac{\pi}{2} - \frac{\alpha}{2}, -\frac{\pi}{2}]$

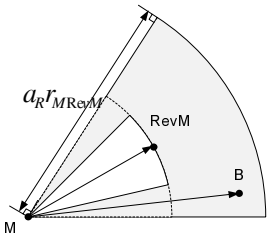

Fig. 4. An illustration for B to be interfered when $r_{MB} < R$.

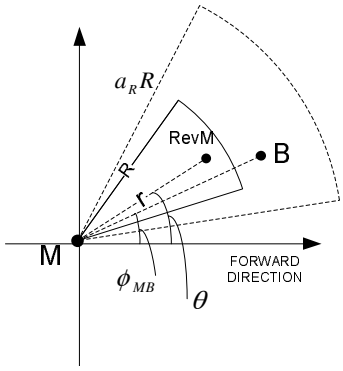

Fig. 5. An illustration for B to be interfered by M in MFR.

- $0 < r_{MB} < a_R \cdot r_M$
- $|\theta - \phi_{MB}| \leq \frac{\alpha}{2}$

The argument is similar to that in Section III-B.2. The only difference is that B is within the maximum transmission range of M for this case. The upper and lower bounds of r_{MB} are changed to R and zero, respectively.

When $\alpha \in (0, \pi]$, $P_r(I, Div(4))$ can be evaluated as (13), shown in the second next page.

When $\alpha \in (\pi, 2\pi]$, $P_r(I, Div(4))$ can be evaluated as (14), shown in the second next page.

C. Probability of Interference for MFR

In MFR, the transmitter chooses a node with the largest forward progress for transmission. As shown in Fig. 5, it will use the fixed transmission radius *R* regardless of the position for the intended receiver. Thus, MFR uses less number of hops to relay packets, but the probability of interference for MFR is greater than that for NFP.

The maximum interference range of M is divided into four divisions as discussed in Section III-B. The probability of interference, $P_r(I)$, can be computed as follows:

$$P_r(I) = \sum_{i=1}^{4} P_r(I, Div(i)) \tag{15}$$

where $P_r(I, Div(i))$ denotes the probability that B is in Division i, where i = 1, 2, 3, 4.

By [6], the probability density function of a receiver's position using MFR can be computed as:

$$f_{r,\theta}^{MFR}(r_0, \theta_0) = \frac{\lambda r_0 e^{-\lambda A_Z}}{1 - e^{-\frac{N}{2}}}, r_0 \in (0, R], \theta_0 \in [-\frac{\pi}{2}, \frac{\pi}{2}] \tag{16}$$

where $A_Z = R^2 \cdot [\cos^{-1}(\frac{r_0 \cos\theta_0}{R}) - \frac{r_0 \cos\theta_0}{R} \cdot \sqrt{1 - (\frac{r_0 \cos\theta_0}{R})^2}]$. Note that the transmission radius of M is always equal to R for MFR. Thus, $r_M = R$.

$$\begin{aligned}P_r(I,Div(2)) &= P_r(M+,B\in\Psi_{M\to RevM},Div(2)) = P_r(M+)\cdot P_r(B\in\Psi_{M\to RevM}|Div(2),M+)\cdot P_r(Div(2)|M+)\\ &= P_r(M+)\cdot[\int_R^{a_RR}\int_{\frac{\pi}{2}}^{\frac{\pi}{2}+\frac{\alpha}{2}} f_{r_{MB},\phi_{MB}}(r_{mb},\phi_{mb})\cdot P_r(B\in\Psi_{M\to RevM}|Div(2),M+)d\phi_{mb}dr_{mb}\\ &\quad+\int_R^{a_RR}\int_{-\frac{\pi}{2}-\frac{\alpha}{2}}^{-\frac{\pi}{2}} f_{r_{MB},\phi_{MB}}(r_{mb},\phi_{mb})\cdot P_r(B\in\Psi_{M\to RevM}|Div(2),M+)d\phi_{mb}dr_{mb}]\\ &= \frac{\lambda}{\pi(a_RR)^2}\cdot(\int_R^{a_RR}\int_{\frac{\pi}{2}}^{\frac{\pi}{2}+\frac{\alpha}{2}}\int_{\phi_{mb}-\frac{\alpha}{2}}^{\frac{\pi}{2}}\int_{\frac{r_{mb}}{a_R}}^{R} r_{mb}r_0e^{-\frac{\lambda\pi r_0^2}{2}}dr_0d\theta_0d\phi_{mb}dr_{mb}\\ &\quad+\int_R^{a_RR}\int_{-\frac{\pi}{2}-\frac{\alpha}{2}}^{-\frac{\pi}{2}}\int_{-\frac{\pi}{2}}^{\frac{\alpha}{2}+\phi_{mb}}\int_{\frac{r_{mb}}{a_R}}^{R} r_{mb}r_0e^{-\frac{\lambda\pi r_0^2}{2}}dr_0d\theta_0d\phi_{mb}dr_{mb}) \qquad (9)\end{aligned}$$

$$P_r(B\in\Psi_{M\to RevM}|Div(2),M+) = \int_{\phi_{mb}-\frac{\alpha}{2}}^{\frac{\pi}{2}}\int_{\frac{r_{mb}}{a_R}}^{R} f_{r,\theta}^{NFP}(r_0,\theta_0)dr_0d\theta_0 + \int_{-\frac{\pi}{2}}^{\frac{\alpha}{2}+\phi_{mb}}\int_{\frac{r_{mb}}{a_R}}^{R} f_{r,\theta}^{NFP}(r_0,\theta_0)dr_0d\theta_0 \qquad (10)$$

$$\begin{aligned}&P_r(I,Div(2))\\ =\;& P_r(M+,B\in\Psi_{M\to RevM},Div(2)) = P_r(M+)\cdot P_r(B\in\Psi_{M\to RevM}|Div(2),M+)\cdot P_r(Div(2)|M+)\\ =\;& \frac{\lambda}{\pi(a_RR)^2}\cdot[\int_R^{a_RR}\int_{\frac{\pi}{2}}^{\frac{\pi}{2}+\frac{\alpha}{2}} r_{mb}\cdot(\int_{\phi_{mb}-\frac{\alpha}{2}}^{\frac{\pi}{2}}\int_{\frac{r_{mb}}{a_R}}^{R} r_0e^{-\frac{\lambda\pi r_0^2}{2}}dr_0d\theta_0+\int_{-\frac{\pi}{2}}^{\frac{\alpha}{2}+\phi_{mb}}\int_{\frac{r_{mb}}{a_R}}^{R} r_0e^{-\frac{\lambda\pi r_0^2}{2}}dr_0d\theta_0)d\phi_{mb}dr_{mb}\\ &+\int_R^{a_RR}\int_{-\frac{\pi}{2}-\frac{\alpha}{2}}^{-\frac{\pi}{2}} r_{mb}\cdot(\int_{-\frac{\pi}{2}}^{\frac{\alpha}{2}+\phi_{mb}}\int_{\frac{r_{mb}}{a_R}}^{R} r_0e^{-\frac{\lambda\pi r_0^2}{2}}dr_0d\theta_0+\int_{\phi_{mb}-\frac{\alpha}{2}}^{\frac{\pi}{2}}\int_{\frac{r_{mb}}{a_R}}^{R} r_0e^{-\frac{\lambda\pi r_0^2}{2}}dr_0d\theta_0)d\phi_{mb}dr_{mb}] \qquad (11)\end{aligned}$$

$$\begin{aligned}P_r(I,Div(3)) &= P_r(M+,B\in\Psi_{M\to RevM},Div(3)) = P_r(B\in\Psi_{M\to RevM}|Div(3))\cdot P_r(Div(3))\\ &= \int_0^R\int_{-\frac{\pi}{2}}^{\frac{\pi}{2}} f_{r_{MB},\phi_{MB}}(r_{mb},\phi_{mb})\cdot P_r(B\in\Psi_{M\to RevM}|Div(3))d\phi_{mb}dr_{mb}\\ &= \frac{\lambda}{\pi(a_RR)^2(1-e^{-\frac{N}{2}})}\cdot\int_0^R\int_{-\frac{\pi}{2}}^{\frac{\pi}{2}}\int_{\frac{r_{mb}}{a_R}}^{r_{mb}}\int_{\phi_1}^{\phi_2} r_{mb}\cdot r_0\cdot e^{-\frac{\lambda\pi r_0^2}{2}}d\theta_0dr_0d\phi_{mb}dr_{mb} \qquad (12)\end{aligned}$$

Since r_M is always equal to R, the interference radius of M is a_RR irrespective of where $RevM$ is. r can be any value within $(0,R]$. Following arguments similar to those in Section III-B,

$$\begin{aligned}&P_r(I,Div(1))\\ =&P_r(M+,B\in\Psi_{M\to RevM},Div(1))\\ =&P_r(M+)\cdot P_r(B\in\Psi_{M\to RevM},Div(1)|M+)\\ =&(1-e^{-\frac{N}{2}})\cdot\int_R^{a_RR}\int_{-\frac{\pi}{2}}^{\frac{\pi}{2}} f_{r_{MB},\phi_{MB}}(r_{mb},\phi_{mb})\\ &\cdot P_r(B\in\Psi_{M\to RevM}|Div(1),M+)d\phi_{mb}dr_{mb}\\ =&\frac{\lambda}{\pi(a_RR)^2}\cdot\int_R^{a_RR}\int_{-\frac{\pi}{2}}^{\frac{\pi}{2}}\int_0^R\int_{\phi_1}^{\phi_2} r_{mb}\cdot r_0\\ &\cdot e^{-\lambda A_Z}d\theta_0dr_0d\phi_{mb}dr_{mb}\end{aligned} \qquad (17)$$

where $\phi_1 = max\{(\phi_{mb}-\frac{\alpha}{2}),-\frac{\pi}{2}\}$ and $\phi_2 = min\{(\phi_{mb}+\frac{\alpha}{2}),\frac{\pi}{2}\}$. Note that the boundary effects can be handled similarly as in NFP.

$P_r(I,Div(2))$, $P_r(I,Div(3))$, and $P_r(I,Div(4))$ can be determined as (18), (19), and (20), respectively, shown in the next two pages, where $\phi_1 = max\{(\phi_{mb}-\frac{\alpha}{2}),-\frac{\pi}{2}\}$ and $\phi_2 = min\{(\phi_{mb}+\frac{\alpha}{2}),\frac{\pi}{2}\}$.

D. Probability of Interference for MVR

In MVR, the transmitter chooses a node with the largest forward progress for transmission. The transmission radius is set to be equal to the distance between the transmitter and the intended receiver.

The maximum interference range of M is divided into four divisions as discussed in Section III-B. The probability of interference, $P_r(I)$, can be computed as follows:

$$P_r(I) = \sum_{i=1}^{4} P_r(I,Div(i)) \qquad (21)$$

where $P_r(I,Div(i))$ denotes the probability that B is in Division i, where i = 1, 2, 3, 4.

By [6], the probability density function of a receiver's position in MVR is the same as that in MFR:

$$f_{r,\theta}^{MVR}(r_0,\theta_0) = \frac{\lambda r_0e^{-\lambda A_Z}}{1-e^{-\frac{N}{2}}}, r_0\in(0,R], \theta_0\in[-\frac{\pi}{2},\frac{\pi}{2}] \qquad (22)$$

where $A_Z = R^2\cdot[\cos^{-1}(\frac{r_0\cos\theta_0}{R}) - \frac{r_0\cos\theta_0}{R}\cdot\sqrt{1-(\frac{r_0\cos\theta_0}{R})^2}]$. Note that the transmission radius r_M is equal to r in MVR. Thus, $r_M = r$.

$$\begin{aligned}
P_r(I,Div(4)) &= P_r(M+,B\in\Psi_{M\to RevM},Div(4)) = P_r(M+)\cdot P_r(B\in\Psi_{M\to RevM}|Div(4),M+)\cdot P_r(Div(4)|M+)\\
&= P_r(M+)\cdot[\int_0^R\int_{\frac{\pi}{2}}^{\frac{\pi}{2}+\frac{\alpha}{2}} f_{r_{MB},\phi_{MB}}(r_{mb},\phi_{mb})\cdot P_r(B\in\Psi_{M\to RevM}|Div(4),M+)d\phi_{mb}dr_{mb}\\
&\quad+\int_0^R\int_{-\frac{\pi}{2}-\frac{\alpha}{2}}^{-\frac{\pi}{2}} f_{r_{MB},\phi_{MB}}(r_{mb},\phi_{mb})\cdot P_r(B\in\Psi_{M\to RevM}|Div(4),M+)d\phi_{mb}dr_{mb}]\\
&= \frac{\lambda}{\pi(a_RR)^2}\cdot(\int_0^R\int_{\frac{\pi}{2}}^{\frac{\pi}{2}+\frac{\alpha}{2}}\int_{\phi_{mb}-\frac{\alpha}{2}}^{\frac{\pi}{2}}\int_{\frac{r_{mb}}{a_R}}^{R} r_{mb}r_0e^{-\frac{\lambda\pi r_0^2}{2}}dr_0d\theta_0d\phi_{mb}dr_{mb}\\
&\quad+\int_0^R\int_{-\frac{\pi}{2}-\frac{\alpha}{2}}^{-\frac{\pi}{2}}\int_{-\frac{\pi}{2}}^{\frac{\alpha}{2}+\phi_{mb}}\int_{\frac{r_{mb}}{a_R}}^{R} r_{mb}r_0e^{-\frac{\lambda\pi r_0^2}{2}}dr_0d\theta_0d\phi_{mb}dr_{mb}) \qquad (13)
\end{aligned}$$

$$\begin{aligned}
P_r(I,Div(4)) &= P_r(M+,B\in\Psi_{M\to RevM},Div(4)) = P_r(M+)\cdot P_r(B\in\Psi_{M\to RevM}|Div(4),M+)\cdot P_r(Div(4)|M+)\\
&= \frac{\lambda}{\pi(a_RR)^2}\cdot[\int_0^R\int_{\frac{\pi}{2}}^{\frac{\pi}{2}+\frac{\alpha}{2}} r_{mb}\cdot(\int_{\phi_{mb}-\frac{\alpha}{2}}^{\frac{\pi}{2}}\int_{\frac{r_{mb}}{a_R}}^{R} r_0e^{-\frac{\lambda\pi r_0^2}{2}}dr_0d\theta_0+\int_{-\frac{\pi}{2}}^{\frac{\alpha}{2}+\phi_{mb}}\int_{\frac{r_{mb}}{a_R}}^{R} r_0e^{-\frac{\lambda\pi r_0^2}{2}}dr_0d\theta_0)d\phi_{mb}dr_{mb}\\
&\quad+\int_0^R\int_{-\frac{\pi}{2}-\frac{\alpha}{2}}^{-\frac{\pi}{2}} r_{mb}\cdot(\int_{-\frac{\pi}{2}}^{\frac{\alpha}{2}+\phi_{mb}}\int_{\frac{r_{mb}}{a_R}}^{R} r_0e^{-\frac{\lambda\pi r_0^2}{2}}dr_0d\theta_0+\int_{\phi_{mb}-\frac{\alpha}{2}}^{\frac{\pi}{2}}\int_{\frac{r_{mb}}{a_R}}^{R} r_0e^{-\frac{\lambda\pi r_0^2}{2}}dr_0d\theta_0)d\phi_{mb}dr_{mb}] \qquad (14)
\end{aligned}$$

$$P_r(I,Div(2)) = \begin{cases}
\frac{\lambda}{\pi(a_RR)^2}\cdot(\int_R^{a_RR}\int_{\frac{\pi}{2}}^{\frac{\pi}{2}+\frac{\alpha}{2}}\int_{\phi_{mb}-\frac{\alpha}{2}}^{\frac{\pi}{2}}\int_0^R r_{mb}r_0e^{-\lambda A_Z}dr_0d\theta_0d\phi_{mb}dr_{mb}\\
+\int_R^{a_RR}\int_{-\frac{\pi}{2}-\frac{\alpha}{2}}^{-\frac{\pi}{2}}\int_{-\frac{\pi}{2}}^{\frac{\alpha}{2}+\phi_{mb}}\int_0^R r_{mb}r_0e^{-\lambda A_Z}dr_0d\theta_0d\phi_{mb}dr_{mb}) & \alpha\in(0,\pi]\\
\frac{\lambda}{\pi(a_RR)^2}\cdot[\int_R^{a_RR}\int_{\frac{\pi}{2}}^{\frac{\pi}{2}+\frac{\alpha}{2}} r_{mb}\cdot(\int_{\phi_{mb}-\frac{\alpha}{2}}^{\frac{\pi}{2}}\int_0^R r_0e^{-\lambda A_Z}dr_0d\theta_0\\
+\int_{-\frac{\pi}{2}}^{\frac{\alpha}{2}+\phi_{mb}}\int_0^R r_0e^{-\lambda A_Z}dr_0d\theta_0)d\phi_{mb}dr_{mb}+\int_R^{a_RR}\int_{-\frac{\pi}{2}-\frac{\alpha}{2}}^{-\frac{\pi}{2}} r_{mb}\\
\cdot(\int_{-\frac{\pi}{2}}^{\frac{\alpha}{2}+\phi_{mb}}\int_0^R r_0e^{-\lambda A_Z}dr_0d\theta_0+\int_{\phi_{mb}-\frac{\alpha}{2}}^{\frac{\pi}{2}}\int_0^R r_0e^{-\lambda A_Z}dr_0d\theta_0)d\phi_{mb}dr_{mb}] & \alpha\in(\pi,2\pi]
\end{cases} \qquad (18)$$

$$\begin{aligned}
P_r(I,Div(3)) &= P_r(B\in\Psi_{M\to RevM},Div(3)) = \int_0^R\int_{-\frac{\pi}{2}}^{\frac{\pi}{2}} f_{r_{MB},\phi_{MB}}(r_{mb},\phi_{mb})\cdot P_r(B\in\Psi_{M\to RevM}|Div(3))d\phi_{mb}dr_{mb}\\
&= \frac{\lambda}{\pi(a_RR)^2(1-e^{-\frac{N}{2}})}\cdot\int_0^R\int_{-\frac{\pi}{2}}^{\frac{\pi}{2}}\int_0^R\int_{\phi_1}^{\phi_2} r_{mb}\cdot r_0\cdot e^{-\lambda A_Z}d\theta_0dr_0d\phi_{mb}dr_{mb} \qquad (19)
\end{aligned}$$

Following arguments similar to those in Section III-B,

$$\begin{aligned}
&P_r(I,Div(1))\\
=&P_r(M+,B\in\Psi_{M\to RevM},Div(1))\\
=&P_r(M+)\cdot P_r(B\in\Psi_{M\to RevM},Div(1)|M+)\\
=&P_r(M+)\cdot\int_R^{a_RR}\int_{-\frac{\pi}{2}}^{\frac{\pi}{2}} f_{r_{MB},\phi_{MB}}(r_{mb},\phi_{mb})\\
&\cdot P_r(B\in\Psi_{M\to RevM}|Div(1),M+)d\phi_{mb}dr_{mb}\\
=&\frac{\lambda}{\pi(a_RR)^2}\cdot\int_R^{a_RR}\int_{-\frac{\pi}{2}}^{\frac{\pi}{2}}\int_{\frac{r_{mb}}{a_R}}^{R}\int_{\phi_1}^{\phi_2} r_{mb}\cdot r_0\\
&\cdot e^{-\lambda A_Z}d\theta_0dr_0d\phi_{mb}dr_{mb}
\end{aligned} \qquad (23)$$

where $\phi_1 = max\{(\phi_{mb}-\frac{\alpha}{2}),-\frac{\pi}{2}\}$ and $\phi_2 = min\{(\phi_{mb}+\frac{\alpha}{2}),\frac{\pi}{2}\}$.

$P_r(I,Div(2))$ can be computed as (24), shown in the next page.

$$\begin{aligned}
&P_r(I,Div(3))\\
=&P_r(B\in\Psi_{M\to RevM},Div(3))\\
=&\int_0^R\int_{-\frac{\pi}{2}}^{\frac{\pi}{2}} f_{r_{MB},\phi_{MB}}(r_{mb},\phi_{mb})\\
&\cdot P_r(B\in\Psi_{M\to RevM}|Div(3))d\phi_{mb}dr_{mb}\\
=&\frac{\lambda}{\pi(a_RR)^2(1-e^{-\frac{N}{2}})}\\
&\cdot\int_0^R\int_{-\frac{\pi}{2}}^{\frac{\pi}{2}}\int_{\frac{r_{mb}}{a_R}}^{R}\int_{\phi_1}^{\phi_2} r_{mb}\cdot r_0\cdot e^{-\lambda A_Z}d\theta_0dr_0d\phi_{mb}dr_{mb}
\end{aligned} \qquad (25)$$

where $\phi_1 = max\{(\phi_{mb}-\frac{\alpha}{2}),-\frac{\pi}{2}\}$ and $\phi_2 = min\{(\phi_{mb}+\frac{\alpha}{2}),\frac{\pi}{2}\}$.

$P_r(I,Div(4))$ can be computed as (26), shown in the next page.

$$P_r(I,Div(4))=\begin{cases}\frac{\lambda}{\pi(a_RR)^2}\cdot(\int_0^R\int_{\frac{\pi}{2}}^{\frac{\pi}{2}+\frac{\alpha}{2}}\int_{\phi_{mb}-\frac{\alpha}{2}}^{\frac{\pi}{2}}\int_0^R r_{mb}r_0e^{-\lambda A_Z}dr_0d\theta_0d\phi_{mb}dr_{mb} & \\ +\int_0^R\int_{-\frac{\pi}{2}-\frac{\alpha}{2}}^{-\frac{\pi}{2}}\int_{-\frac{\pi}{2}}^{\frac{\alpha}{2}+\phi_{mb}}\int_0^R r_{mb}r_0e^{-\lambda A_Z}dr_0d\theta_0d\phi_{mb}dr_{mb}) & \alpha\in(0,\pi]\\ \frac{\lambda}{\pi(a_RR)^2}\cdot[\int_0^R\int_{\frac{\pi}{2}}^{\frac{\pi}{2}+\frac{\alpha}{2}}r_{mb}\cdot(\int_{\phi_{mb}-\frac{\alpha}{2}}^{\frac{\pi}{2}}\int_0^R r_0e^{-\lambda A_Z}dr_0d\theta_0 & \\ +\int_{-\frac{\pi}{2}}^{\frac{\alpha}{2}+\phi_{mb}}\int_0^R r_0e^{-\lambda A_Z}dr_0d\theta_0)d\phi_{mb}dr_{mb}+\int_0^R\int_{-\frac{\pi}{2}-\frac{\alpha}{2}}^{-\frac{\pi}{2}}r_{mb} & \\ \cdot(\int_{-\frac{\pi}{2}}^{\frac{\alpha}{2}+\phi_{mb}}\int_0^R r_0e^{-\lambda A_Z}dr_0d\theta_0+\int_{\phi_{mb}-\frac{\alpha}{2}}^{\frac{\pi}{2}}\int_0^R r_0e^{-\lambda A_Z}dr_0d\theta_0)d\phi_{mb}dr_{mb}] & \alpha\in(\pi,2\pi]\end{cases}\tag{20}$$

$$P_r(I,Div(2))=\begin{cases}\frac{\lambda}{\pi(a_RR)^2}\cdot(\int_R^{a_RR}\int_{\frac{\pi}{2}}^{\frac{\pi}{2}+\frac{\alpha}{2}}\int_{\phi_{mb}-\frac{\alpha}{2}}^{\frac{\pi}{2}}\int_{\frac{r_{mb}}{a_R}}^R r_{mb}r_0e^{-\lambda A_Z}dr_0d\theta_0d\phi_{mb}dr_{mb} & \\ +\int_R^{a_RR}\int_{-\frac{\pi}{2}-\frac{\alpha}{2}}^{-\frac{\pi}{2}}\int_{-\frac{\pi}{2}}^{\frac{\alpha}{2}+\phi_{mb}}\int_{\frac{r_{mb}}{a_R}}^R r_{mb}r_0e^{-\lambda A_Z}dr_0d\theta_0d\phi_{mb}dr_{mb}) & \alpha\in(0,\pi]\\ \frac{\lambda}{\pi(a_RR)^2}\cdot[\int_R^{a_RR}\int_{\frac{\pi}{2}}^{\frac{\pi}{2}+\frac{\alpha}{2}}r_{mb}\cdot(\int_{\phi_{mb}-\frac{\alpha}{2}}^{\frac{\pi}{2}}\int_{\frac{r_{mb}}{a_R}}^R r_0e^{-\lambda A_Z}dr_0d\theta_0 & \\ +\int_{-\frac{\pi}{2}}^{\frac{\alpha}{2}+\phi_{mb}}\int_{\frac{r_{mb}}{a_R}}^R r_0e^{-\lambda A_Z}dr_0d\theta_0)d\phi_{mb}dr_{mb}+\int_R^{a_RR}\int_{-\frac{\pi}{2}-\frac{\alpha}{2}}^{-\frac{\pi}{2}}r_{mb} & \\ \cdot(\int_{-\frac{\pi}{2}}^{\frac{\alpha}{2}+\phi_{mb}}\int_{\frac{r_{mb}}{a_R}}^R r_0e^{-\lambda A_Z}dr_0d\theta_0+\int_{\phi_{mb}-\frac{\alpha}{2}}^{\frac{\pi}{2}}\int_{\frac{r_{mb}}{a_R}}^R r_0e^{-\lambda A_Z}dr_0d\theta_0)d\phi_{mb}dr_{mb}] & \alpha\in(\pi,2\pi]\end{cases}\tag{24}$$

$$P_r(I,Div(4))=\begin{cases}\frac{\lambda}{\pi(a_RR)^2}\cdot(\int_0^R\int_{\frac{\pi}{2}}^{\frac{\pi}{2}+\frac{\alpha}{2}}\int_{\phi_{mb}-\frac{\alpha}{2}}^{\frac{\pi}{2}}\int_{\frac{r_{mb}}{a_R}}^R r_{mb}r_0e^{-\lambda A_Z}dr_0d\theta_0d\phi_{mb}dr_{mb} & \\ +\int_0^R\int_{-\frac{\pi}{2}-\frac{\alpha}{2}}^{-\frac{\pi}{2}}\int_{-\frac{\pi}{2}}^{\frac{\alpha}{2}+\phi_{mb}}\int_{\frac{r_{mb}}{a_R}}^R r_{mb}r_0e^{-\lambda A_Z}dr_0d\theta_0d\phi_{mb}dr_{mb}) & \alpha\in(0,\pi]\\ \frac{\lambda}{\pi(a_RR)^2}\cdot[\int_0^R\int_{\frac{\pi}{2}}^{\frac{\pi}{2}+\frac{\alpha}{2}}r_{mb}\cdot(\int_{\phi_{mb}-\frac{\alpha}{2}}^{\frac{\pi}{2}}\int_{\frac{r_{mb}}{a_R}}^R r_0e^{-\lambda A_Z}dr_0d\theta_0 & \\ +\int_{-\frac{\pi}{2}}^{\frac{\alpha}{2}+\phi_{mb}}\int_{\frac{r_{mb}}{a_R}}^R r_0e^{-\lambda A_Z}dr_0d\theta_0)d\phi_{mb}dr_{mb} & \\ +\int_0^R\int_{-\frac{\pi}{2}-\frac{\alpha}{2}}^{-\frac{\pi}{2}}r_{mb}\cdot(\int_{-\frac{\pi}{2}}^{\frac{\alpha}{2}+\phi_{mb}}\int_{\frac{r_{mb}}{a_R}}^R r_0e^{-\lambda A_Z}dr_0d\theta_0 & \\ +\int_{\phi_{mb}-\frac{\alpha}{2}}^{\frac{\pi}{2}}\int_{\frac{r_{mb}}{a_R}}^R r_0e^{-\lambda A_Z}dr_0d\theta_0)d\phi_{mb}dr_{mb}] & \alpha\in(\pi,2\pi]\end{cases}\tag{26}$$

E. Special Case

The results in [6] correspond to a special case of the analytical model in this paper when $\beta=2\pi$, $a_R=1$, and $a_\beta=1$. That is, the interference range is a circle and equal to the transmission range.

Taking $\beta=2\pi$ and $a_R=a_\beta=1$ in our model, we obtain the same results as in [6] for MFR and MVR. However, the results in [5] for NFP are different from ours. The following argument for NFP has been made in [6]:

When B is in M's forward direction, M can always find a receiver. Interference will take place if the transmission radius of M, r_M, is greater than the distance between M and B, r_{MB}. The probability of interference is computed as:

$$P_r(B \text{ gets interfered by } M)=\int_{r_{MB}}^R f_r(r_0)dr_0 \tag{27}$$

However, in NFP, M always transmits to the nearest neighbour which can provide positive forward progress. Therefore, when B is in M's forward semicircle, it is not possible that r_M would exceed r_{MB}. In other words, since $r_M=r$, r cannot fall into the range of $[r_{MB},R]$. The problem can be solved by taking the interference range into consideration. The probability of interference can be calculated by $\int_{\frac{r_{MB}}{a_R}}^{r_{MB}} f_r(r_0)dr_0$, where $r_{MB}>r\geq\frac{r_{MB}}{a_R}$. One may refer to Section III-B.3 for details.

F. Discussion on Heterogeneous Network Model

In this paper, all nodes in the network are assumed to be distributed as a two-dimensional Poisson point process with a constant density λ. This homogeneous network model is widely employed in the literature of ad hoc networks [2], [6], [9], [11]. Our proposed analytical model can be extended to heterogeneous networks as well. Denote by $\lambda(r_d,\theta_d)$ the node density for a heterogenous network, where (r_d,θ_d) is the polar coordinates of a node with respect to the centre of the network $O(0,0)$. The joint probability density function of r_{MB} and ϕ_{MB}, where (r_{MB},ϕ_{MB}) is the polar coordinates of a receiver B with respect to its neighbour M, is $f_{r_{MB},\phi_{MB}}(r_{mb},\phi_{mb},\lambda'(r_{mb},\phi_{mb}))$. Suppose (r_M,θ_M) is the polar coordinates of M with respect to O. By conducting coordinate shift, (r_{MB},θ_{MB}) in the coordinate system where O is the origin can be expressed as $(\sqrt{r_{MB}^2+r_M^2-2r_{MB}r_M\cos(\phi_{MB}-\theta_M)}$, $\tan^{-1}(\frac{r_{MB}\sin\phi_{MB}-r_M\sin\theta_M}{r_{MB}\cos\phi_{MB}-r_M\cos\theta_M}))$, we can get:

$$\begin{aligned}&\lambda'(r_{MB},\phi_{MB})\\ =&\lambda(\sqrt{r_{MB}^2+r_M^2-2r_{MB}r_M\cos(\phi_{MB}-\theta_M)},\\ &\tan^{-1}(\frac{r_{MB}\sin\phi_{MB}-r_M\sin\theta_M}{r_{MB}\cos\phi_{MB}-r_M\cos\theta_M}))\end{aligned}\tag{28}$$

Similarly, the probability density function (corresponding to (7)) of a receiver's position for a transmission is $f_{r,\theta}^X(r_0,\theta_0,\lambda''(r_0,\theta_0))$, where (r_0,θ_0) is the polar coordinates of the receiver with respect to its transmitter M, $r_0\in(0,R]$, $\theta_0\in[-\frac{\pi}{2},\frac{\pi}{2}]$, and X = NFP, MFR, MVR for the NFP, MFR, and MVR strategies, respectively. By conducting coordinate shift, (r_0,θ_0) in the coordinate system where O is the origin can be written as $(\sqrt{r_0^2+r_M^2-2r_0r_M\cos(\phi_0-\theta_M)}$,

$\tan^{-1}(\frac{r_0 \sin\phi_0 - r_M \sin\theta_M}{r_0 \cos\phi_0 - r_M \cos\theta_M})$), we can get:

$$\begin{aligned}\lambda^{''}(r_0,\phi_0) =& \lambda(\sqrt{r_0^2 + r_M^2 - 2r_0 r_M \cos(\phi_0 - \theta_M)}, \\ & \tan^{-1}(\frac{r_0 \sin\phi_0 - r_M \sin\theta_M}{r_0 \cos\phi_0 - r_M \cos\theta_M}))\end{aligned} \tag{29}$$

We divide the maximum interference range into four divisions and get the probability of interference using (6). For heterogeneous networks, the interference probability can be calculated as:

$$\begin{aligned}& P_r(I, Div(i)) \\ =& P_r(M+, B \in \Psi_{M \to RevM}, Div(i)) \\ =& P_r(M+) \cdot P_r(B \in \Psi_{M \to RevM}, Div(i) | M+) \\ =& P_r(M+) \cdot \int \cdots \int_D f_M(r_M, \theta_M) \\ & \cdot f_{r_{MB},\phi_{MB}}(r_{mb}, \phi_{mb}, \lambda^{'}(r_{mb}, \phi_{mb})) \\ & \cdot f^X_{r,\theta}(r_0, \theta_0, \lambda^{''}(r_0, \theta_0)) dr_0 d\theta_0 d\phi_{mb} dr_{mb} dr_M d\theta_M\end{aligned} \tag{30}$$

where $f_M(r_M, \theta_M)$ with the domain of the network under study Ω is the probability density function of the location of M at (r_M, θ_M) with respect to the centre of the network O, and is specific to the network under study, $D = \{(r_M, \theta_M, r_{mb}, \phi_{mb}, r_0, \theta_0) \in \Re^6 : r_M, \theta_M \in \Omega, r_{mb} \in (0, a_R R], \phi_{mb} \in [0, 2\pi), r_0 \in (0, R], \theta_0 \in [-\frac{\pi}{2}, \frac{\pi}{2}]\}$, and i = 1, 2, 3, 4 for the cases when B is in Divisions 1, 2, 3, and 4, respectively. $P_r(M+)$ is the probability that Node M can find an eligible receiver in the forward semicircle and is also subject to the specific node distribution in the network.

IV. Performance Analysis

A. Slotted ALOHA

We assume that all nodes in the network transmit with probability p. I^c is the event that M does not interfere with B. M^t is the event that M transmits, while M^c is the event that it does not transmit.

$$\begin{aligned}P_r(I^c) &= P_r(I^c|M^c) \cdot P(M^c) + P_r(I^c|M^t) \cdot P(M^t) \\ &= 1 \cdot (1-p) + [1 - P_r(I)] \cdot p = 1 - p \cdot P_r(I)\end{aligned} \tag{31}$$

Let N_i be the event that B has i neighbours excluding Node A, and T_{AB} be the event that when there is a transmission from A to B, these i neighbours will not interfere with B. Note that in this paper, the term "neighbour" refers to the node within the maximum interference range which is a circle with radius $a_R R$. Therefore,

$$\begin{aligned}P_r(T_{AB}|N_i) &= (1-p) \cdot [P_r(I^c)]^i \\ &= (1-p) \cdot [1 - p \cdot P_r(I)]^i\end{aligned} \tag{32}$$

Here, we assume that $a_R = a_\beta = 2$ for our study.

For NFP, since B is the nearest node to A that can provide positive forward progress, there is no node in the semicircle between A and B as illustrated in the shaded area E_1 from Fig. 6. We call this area the "excluded region." In this case, we get $E_1 = \frac{1}{2}\pi r^2$.

For MVR and MFR, B is the node which can provide the largest forward progress to A. Thus, the excluded region for these two strategies are illustrated as the dashed region E_2 in Fig. 6, where $E_2 = R^2[\cos^{-1}(\frac{r\cos\theta}{R}) - \frac{r\cos\theta}{R}\sqrt{1 - (\frac{r\cos\theta}{R})^2}]$.

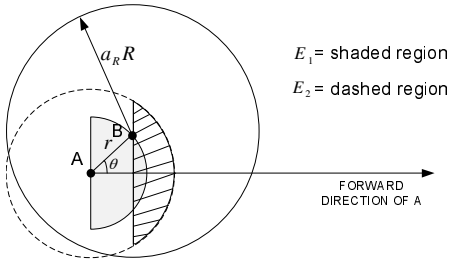

Fig. 6. An illustration for the excluded region.

When $a_R = 2$, the excluded region E is included in the maximum interference range of B. The number of B's neighbours (excluding A) can be calculated as:

$$P_r(N_i|B(r,\theta)) = \frac{\{\lambda[\pi(a_R R)^2 - E]\}^i}{i!} \cdot e^{-\lambda[\pi(a_R R)^2 - E]} \tag{33}$$

where i = 0, 1, 2, ...

Since B is the receiver of A, $r \in (0, R]$, and $\theta \in [-\frac{\pi}{2}, \frac{\pi}{2}]$,

$$\begin{aligned}P_r(T_{AB}) =& \sum_{i=0}^{\infty} P_r(T_{AB}|N_i) P_r(N_i) \\ =& \sum_{i=0}^{\infty} P_r(T_{AB}|N_i) \\ & \cdot \int_0^R \int_{-\frac{\pi}{2}}^{\frac{\pi}{2}} P_r(N_i|B=(r_0,\theta_0)) f^X_{r,\theta}(r_0,\theta_0) d\theta_0 dr_0 \\ =& (1-p) \\ & \cdot \int_0^R \int_{-\frac{\pi}{2}}^{\frac{\pi}{2}} e^{-p \cdot P_r(I) \lambda[\pi(a_R R)^2 - E]} f^X_{r,\theta}(r_0,\theta_0) d\theta_0 dr_0\end{aligned} \tag{34}$$

where X = NFP, MFR, MVR for the NFP, MFR, and MVR strategies, respectively.

We use the following metrics to evaluate the network performance:

S = one-hop throughput = average number of successful transmissions per slot from a node

Z = average forward progress per slot from a node

D = average delay from a transmitter to its final destination in the network

Let $A+$ be the event that A can find a receiver for the transmission, and A^t the event that A transmits. Therefore, the one-hop throughput at Node A can be computed as:

$$S = P_r(A+) \cdot P_r(A^t) \cdot P_r(T_{AB}) = (1 - e^{-\frac{N}{2}}) \cdot p \cdot P_r(T_{AB}) \tag{35}$$

The forward progress is equal to $r\cos\theta$, where r and θ are the transmission radius and angle of A, respectively. We can get the average forward progress Z by inserting $r\cos\theta$ into the above integral:

$$\begin{aligned}Z =& (1 - e^{-\frac{N}{2}}) \cdot p \cdot (1-p) \\ & \cdot \int_0^R \int_{-\frac{\pi}{2}}^{\frac{\pi}{2}} e^{-pP_r(I)\lambda[\pi(a_R R)^2 - E]} r_0 \cos\theta_0 f^X_{r,\theta}(r_0,\theta_0) d\theta_0 dr_0\end{aligned} \tag{36}$$

The expected delay due to interference or no relay node found is calculated as:

$$D = \frac{L_{SD}}{Z} \cdot TD \tag{37}$$

where L_{SD} is the average distance between the source and the destination of a message, and *TD* is the duration of a time slot. Hence, $\frac{L_{SD}}{Z}$ represents the average number of hops between them.

B. Slotted CSMA/CA-Like Protocol

Suppose Node A intends to send and B is its immediate relay or the final destination. Let N_j be the event that B has j neighbours excluding A. In m-slot1, A sends a RTS packet to B with probability p. Let R_{RTS} be the event that B successfully receives a RTS packet from A. That is, when A transmits the RTS packet to B, these j neighbours will not interfere with B. Thus,

$$\begin{aligned}
&P_r(R_{RTS}) \\
=&\sum_{j=0}^{\infty} P_r(R_{RTS}|N_j) \cdot P_r(N_j) \\
=&\sum_{j=0}^{\infty} P_r(R_{RTS}|N_j) \\
&\cdot \int_0^R \int_{-\frac{\pi}{2}}^{\frac{\pi}{2}} P_r(N_j|B=(r_0,\theta_0)) \cdot f_{r,\theta}^X(r_0,\theta_0) d\theta_0 dr_0 \\
=&(1-p) \cdot \int_0^R \int_{-\frac{\pi}{2}}^{\frac{\pi}{2}} e^{-pP_r(I)\lambda[\pi(a_R R)^2 - E]} f_{r,\theta}^X(r_0,\theta_0) d\theta_0 dr_0
\end{aligned} \tag{38}$$

where X = NFP, MFR, MVR for the NFP, MFR, and MVR strategies, respectively, E is the area of the excluded region, and N_j is the event that B has j neighbours excluding Node A.

After receiving the RTS packet in m-slot1, Node B replies with a CTS packet to Node A in m-slot2. Let N_k be the event that A has k neighbours excluding B. $P_r(R_{RTS})$ is indeed the probability that a node sends a CTS packet. Let R_{CTS} be the event that Node A successfully receives a CTS packet from Node B. That is, when B sends the CTS packet to A, these k neighbours will not interfere with A. Therefore,

$$\begin{aligned}
&P_r(R_{CTS}|R_{RTS}) \\
=&\sum_{k=0}^{\infty} P_r(R_{CTS}|R_{RTS}, N_k) \cdot P_r(N_k) \\
=&\sum_{k=0}^{\infty} P_r(R_{CTS}|R_{RTS}, N_k) \\
&\cdot \int_0^R \int_{-\frac{\pi}{2}}^{\frac{\pi}{2}} P_r(N_k|B=(r_0,\theta_0)) \cdot f_{r,\theta}^X(r_0,\theta_0) d\theta_0 dr_0 \\
=&[1 - P_r(R_{RTS})] \\
&\cdot \int_0^R \int_{-\frac{\pi}{2}}^{\frac{\pi}{2}} e^{-P_r(R_{RTS}) \cdot P_r(I)\lambda[\pi(a_R R)^2 - E]} \cdot f_{r,\theta}^X(r_0,\theta_0) d\theta_0 dr_0
\end{aligned} \tag{39}$$

since all nodes are slot-synchronized.

Let A^T be the event that Node A transmits the data after receiving a CTS packet from Node B. Hence,

$$\begin{aligned}
&P_r(A^T) \\
=&P_r(R_{RTS} \bigcap R_{CTS}) \\
=&P_r(R_{CTS}|R_{RTS}) \cdot P_r(R_{RTS}) \\
=&(1-p) \cdot [1 - P_r(R_{RTS})] \\
&\cdot \{ \int_0^R \int_{-\frac{\pi}{2}}^{\frac{\pi}{2}} e^{-p \cdot P_r(I)\lambda[\pi(a_R R)^2 - E]} \cdot f_{r,\theta}^X(r_0,\theta_0) d\theta_0 dr_0 \} \\
&\cdot \{ \int_0^R \int_{-\frac{\pi}{2}}^{\frac{\pi}{2}} e^{-P_r(R_{RTS}) \cdot P_r(I)\lambda[\pi(a_R R)^2 - E]} \cdot f_{r,\theta}^X(r_0,\theta_0) d\theta_0 dr_0 \}
\end{aligned} \tag{40}$$

During the data communication period, since $P_r(I)$ is computed based on the relative locations between the node and its neighbours which is independent of the MAC protocol used, $P_r(I)$ is the same as we have discussed in Section III for all of the three strategies: NFP, MFR, and MVR. I^c is the event that M does not interfere with B. M^t is the event that M transmits, while M^c is the event that M does not transmit. Let N_i be the event that Node B has i neighbours excluding Node A, and T_{AB} be the event that when there is a transmission from A to B, these i neighbours will not interfere with B. Therefore,

$$\begin{aligned}
P_r(I^c) &= P_r(I^c|M^c) \cdot P(M^c) + P_r(I^c|M^t) \cdot P(M^t) \\
&= 1 \cdot [1 - P_r(A^T)] + [1 - P_r(I)] \cdot P_r(A^T) \\
&= 1 - P_r(I) \cdot P_r(A^T)
\end{aligned} \tag{41}$$

$$\begin{aligned}
P_r(T_{AB}|N_i) &= [1 - P_r(A^T)] \cdot [P_r(I^c)]^i \\
&= [1 - P_r(A^T)] \cdot [1 - P_r(A^T) \cdot P_r(I)]^i
\end{aligned} \tag{42}$$

$$\begin{aligned}
&P_r(T_{AB}) \\
=&\sum_{i=0}^{\infty} P_r(T_{AB}|N_i) \cdot P_r(N_i) \\
=&\sum_{i=0}^{\infty} P_r(T_{AB}|N_i) \\
&\cdot \int_0^R \int_{-\frac{\pi}{2}}^{\frac{\pi}{2}} P_r(N_i|B=(r_0,\theta_0)) \cdot f_{r,\theta}^X(r_0,\theta_0) d\theta_0 dr_0 \\
=&[1 - P_r(A^T)] \\
&\cdot \int_0^R \int_{-\frac{\pi}{2}}^{\frac{\pi}{2}} e^{-P_r(A^T) \cdot P_r(I)\lambda[\pi(a_R R)^2 - E]} \cdot f_{r,\theta}^X(r_0,\theta_0) d\theta_0 dr_0
\end{aligned} \tag{43}$$

where X = NFP, MFR, MVR for the NFP, MFR, and MVR strategies, respectively.

For the slotted CSMA/CA-like protocol, the one-hop throughput at Node A can be computed as:

$$S = P_r(A+) \cdot P_r(A^T) \cdot P_r(T_{AB}) \tag{44}$$

The forward progress is equal to $r\cos\theta$, where r and θ are the transmission radius and angle of A, respectively. We can get the average forward progress Z by inserting $r\cos\theta$ into

the above integral:

$$\begin{aligned} Z &= (1-e^{-\frac{N}{2}})\cdot P_r(A^T)\cdot[1-P_r(A^T)] \\ &\quad \cdot \int_0^R \int_{-\frac{\pi}{2}}^{\frac{\pi}{2}} e^{-P_r(A^T)\cdot P_r(I)\lambda[\pi(a_R R)^2-E]} \\ &\quad \cdot r_0 \cos\theta_0 f_{r,\theta}^X(r_0,\theta_0) d\theta_0 dr_0 \end{aligned} \quad (45)$$

C. Simulation and Analysis of Results

We have written a computer program in Visual C++ for our simulation study. To validate our analytical model, the occurrences of events within an area with size of $15R \times 15R$ are simulated, where R is the maximum transmission range. Given the same transmission power, by (1), R varies with different values of beam-width. Nodes are distributed according to the two-dimensional Poisson point process. The position of each node is denoted as (x, y), where x and y are uniformly distributed in [0, $15R$]. The network connectivity N varies from one to ten. The number of nodes in the network is $15R \cdot 15R \cdot \frac{N}{\pi R^2} = \frac{225N}{\pi}$.

The simulation setup is described as follows:

- First, the typical nodes, which are nodes located in the $13R \times 13R$ square centred at the middle of the simulated area, are identified, so as to avoid the edge effect. Denote by F the number of typical nodes. In our simulation, we take $L_{SD} = \frac{13R}{\sqrt{3}}$.
- For each origin-destination pair, the next relay for the transmitter is determined according to the transmission strategy of interest. Thus, three sets of simulations corresponding to NFP, MFR, and MVR are performed.
- *Slotted ALOHA*: Each node in the network transmits with probability p. For each transmission from a transmitter to its next relay, every typical node is checked to see whether it is covered by the interference range of this transmission.
  Slotted CSMA/CA-like protocol: Each node in the network transmits directionally an RTS packet with probability p. For each transmission from a transmitter to its next relay, every typical node is checked to see whether it is covered by the interference range of this transmission.
- *Slotted ALOHA*: Those typical nodes, which are not covered by any interference ranges of others, are identified. If the identified typical node is a relay, a transmission to it is said to be successful and the forward progress of this transmission is recorded. Denote by H the number of the typical nodes with successful transmissions.
  Slotted CSMA/CA-like protocol: Those typical nodes, which are not covered by any interference ranges of others, are identified. If the identified typical node is an RTS receiver, it will reply with a CTS packet back to the sender. After that, every CTS receiver is checked to see whether it is covered by the interference range of this transmission. The CTS receivers, which are not covered by any interference ranges of others, are identified. Denote by H the number of these successful nodes.
- *Slotted CSMA/CA-like protocol*: For the data transmission period, only those nodes that successfully receive a CTS packet will transmit data. A relay of each of these nodes is identified. If a relay is not covered by any interference ranges of others, a transmission to it is said to be successful and the forward progress of this transmission is recorded. Denote by $H^{'}$ the number of the typical nodes with successful transmissions.
- *Slotted ALOHA*: The one-hop throughput S is computed as $\frac{H}{F}$.
  Slotted CSMA/CA-like protocol: The one-hop throughput S is computed as $\frac{H^{'}}{F}$.
- *Slotted ALOHA*: Let Z_{sum} be the sum of the recorded forward progresses. The average forward progress per slot of a node, Z, is computed as $\frac{Z_{sum}}{F}$.
  Slotted CSMA/CA-like protocol: The average forward progress per slot of a node, Z, is computed as $\frac{Z_{sum}}{F}$.

For each value of N, p is chosen to maximize $Z\sqrt{\lambda}$, where $Z\sqrt{\lambda}$ is the normalized average progress per slot [6]. The analytical and simulation results for the one-hop throughput, normalized forward progress, and average delay in the network are shown in Figs. 7-14. The analytical results are shown as symbols connected with line segments, whereas the simulation results are shown as the confidence intervals with dots to denote the estimated average values. Each simulated data value is obtained by averaging the results of 100 simulation runs, and the 95% confidence interval is shown on each of the simulated point. The duration of two mini-slots is negligible with respect to the duration of a time slot. For example, in IEEE 802.11, the total length of an RTS packet and a CTS packet corresponds to less than 10% of a data packet. In general, the analytical and simulation results follow similar trends, but there are still some discrepancies between the analytical and simulation results. In Section III-A, we have assumed that neighbours of a node are uniformly distributed in the maximum interference range of that node. However, there is no node in the excluded region but our analytical model has not taken this into account. We believe that this is the main source for the discrepancies between the analytical and simulation results.

The typical value of beam-width adopted for smart antennas falls within $[\frac{\pi}{6}, \frac{2\pi}{3}]$ [14], [17], [19]. Without loss of generality, we use $\frac{\pi}{6}$, $\frac{\pi}{3}$, and $\frac{\pi}{2}$ as the beam-width values used for our study.

In Fig. 7, the one-hop throughput S versus connectivity N in NFP with different values of beam-width β for slotted ALOHA is plotted. S increases at first, but becomes flat or even decreases as N grows. This is because when the network connectivity is low, it is difficult for a node to find a receiver. The network performance is improved when the network connectivity increases. As N grows, however, more network traffic will lead to more interference, thus deteriorating the network performance. However, in NFP, a transmitter chooses the nearest node in its forward semicircle as its receiver. As N increases, the node is inclined to choose a nearer neighbour for transmission. Hence, the interference range becomes smaller. This counterbalances the performance degradation caused by increasing the traffic load due to larger network density. Therefore, the one-hop throughput for NFP becomes more or less the same even when N increases further. As β shrinks from 2π to $\frac{\pi}{6}$, the transmission and interference ranges become smaller. Thus, when $\beta < 2\pi$, the

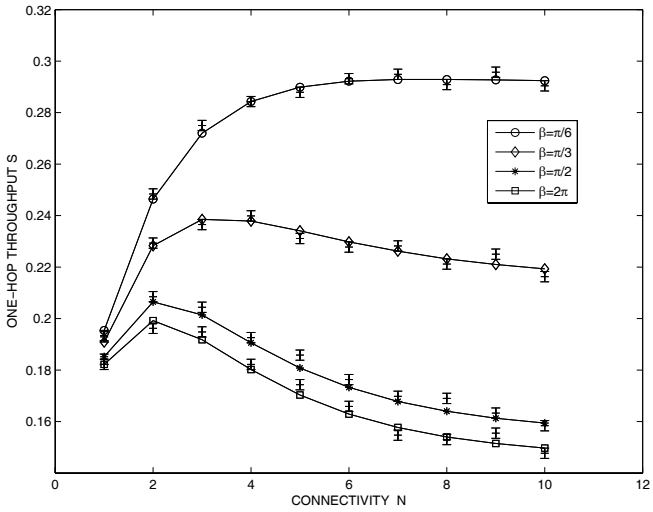

Fig. 7. One-hop throughput S versus connectivity N in NFP for slotted ALOHA.

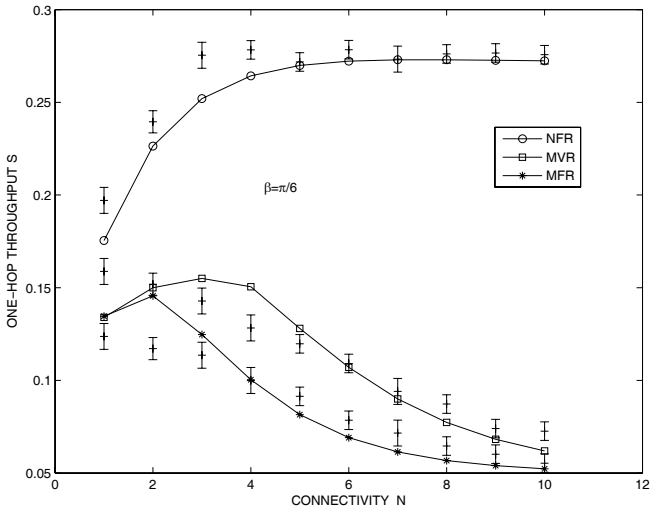

Fig. 8. One-hop throughput S versus connectivity N for slotted ALOHA.

interference can be mitigated by using a smart antenna, which outperforms an omni-directional antenna with respect to the one-hop throughput.

In Fig. 8, the one-hop throughput S versus connectivity N using different strategies for slotted ALOHA is plotted. It can be observed that the one-hop throughput S increases at first and becomes flat for NFP as N increases. For MFR and MVR, the one-hop throughput increases at the beginning but drops when N increases further. In MVR, a transmitter chooses the node with the furthest forward progress as its intended receiver. As N increases, the node is inclined to choose a node with a greater distance for transmission. Hence, the interference range becomes larger. The one-hop throughput of this strategy thus declines with larger network density. For MFR, the transmission range is always equal to R so it yields the greatest possible interference range. Nodes are more likely to get interfered as the network traffic load becomes larger. Since the interference range of MFR is the largest among the three strategies, it yields the worst performance with respect to the one-hop throughput.

We plotted the results of the normalized average progress $Z\sqrt{\lambda}$ for slotted ALOHA in Fig. 9. It is observed that with smart antennas, MFR and MVR have greater $Z\sqrt{\lambda}$ than NFP. When $N < 3$, the differences between the three strategies are comparatively small. This is because when the network is sparse, the nearest forward neighbour is very likely to be the one with the greatest forward progress. However, as N grows, $Z\sqrt{\lambda}$ increases dramatically for MVR and MFR, but it increases and becomes stable for NFP. The reason is that the use of smart antennas can greatly reduce the transmission conflicts in the network.

As we can see from Figs. 8-9, NFP can maintain stable one-hop throughput and normalized average progress $Z\sqrt{\lambda}$ with respect to various node densities. However, for multi-hop applications, since the forward progress is a key measure of performance, NFP behaves worse than MVR and MFR. Meanwhile, compared with MFR, MVR can always yield a

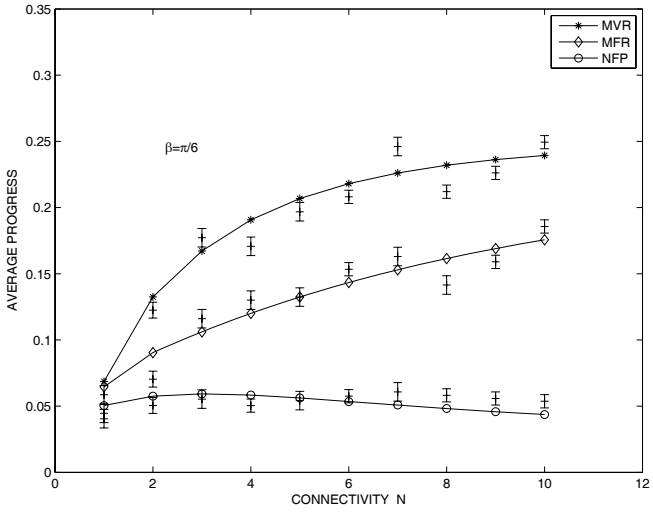

Fig. 9. Normalized average forward progress $Z\sqrt{\lambda}$ versus connectivity N for slotted ALOHA.

better one-hop throughput S, since MVR achieves a smaller interference range for each transmission. Therefore, as we can see in Fig. 9, MVR achieves the best performance in the normalized average forward progress $Z\sqrt{\lambda}$.

In Fig. 10, the average delay D versus connectivity N using different strategies for slotted ALOHA is plotted. We can observe that D decreases at first, and increases as N grows for NFP. NFP has the worst performance in average delay, since a node selects the nearest neighbour on its forward semicircle. It takes more hops than MFR and MVR to relay a packet to the destination. For MFR and MVR, a node selects the farthest neighbour on its forward semicircle. Therefore, as the network connectivity becomes higher, the average delay D decreases. MVR has the best performance in average delay, since it utilizes the power control to limit the interference range in each transmission, while maximizing the effective

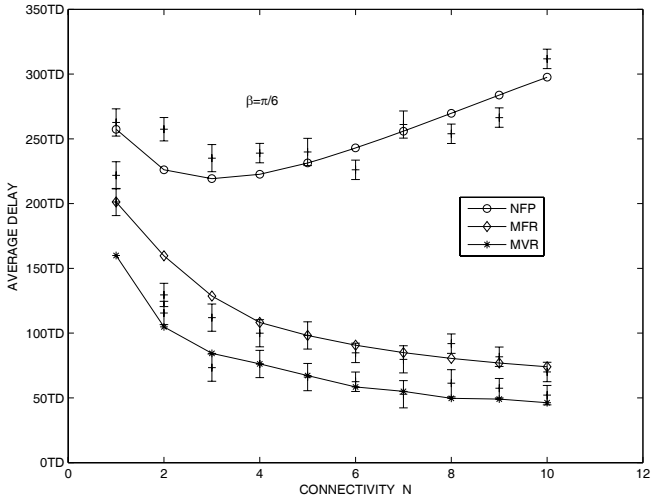

Fig. 10. Average delay D versus connectivity N for slotted ALOHA.

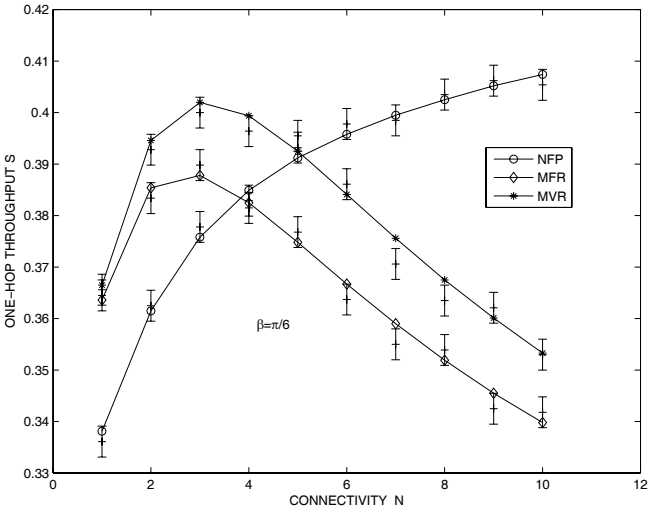

Fig. 12. One-hop throughput S versus connectivity N for CSMA/CA-like protocol.

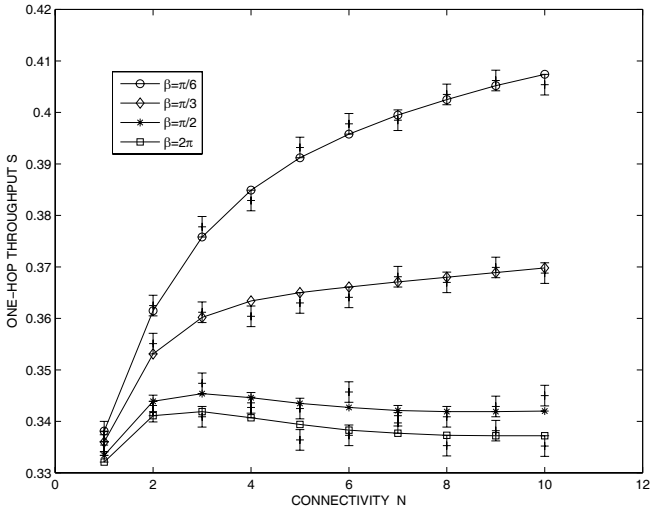

Fig. 11. One-hop throughput S versus connectivity N in NFP for CSMA/CA-like protocol.

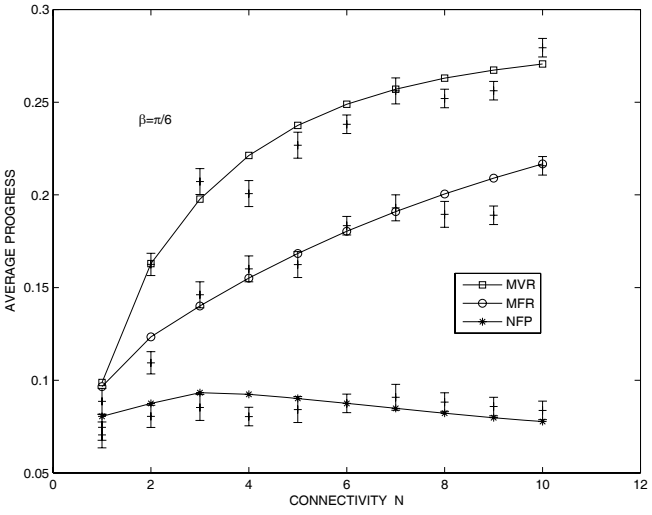

Fig. 13. Normalized average forward progress $Z\sqrt{\lambda}$ versus connectivity N for CSMA/CA-like protocol.

transmission distance by selecting a relay node with the maximum forward progress.

In Fig. 11, the one-hop throughput S versus connectivity N in NFP with different beam-widths for the slotted CSMA/CA-like protocol is shown. It has similar trends as that of the slotted ALOHA protocol in Fig. 7, but with substantially improved performance. This is because by exchanging RTS/CTS packets, nodes can choose a suitable value of $P_r(A^T)$ to transmit data packets which can mitigate interference in the network and improve performance.

In Fig. 12, the one-hop throughput S versus connectivity N using different strategies for the slotted CSMA/CA-like protocol is plotted. It can be seen that the basic trend for each curve is similar to that of the slotted ALOHA protocol in Fig. 8. However, when $N < 5$, the one-hop throughputs of MFR and MVR have better performance over NFP. This is because as N increases, for MFR and MVR, a sender is inclined to choose a node with a larger transmission distance which leads to greater interference range. Since there are more conflicts during the RTS/CTS exchange phase, each node will choose a smaller $P_r(A^T)$ to transmit data. This increases the probability of a successful data transmission, $P_r(T_{AB})$, and thus S, where S is the product of $P_r(A+)$, $P_r(A^T)$, and $P_r(T_{AB})$. For MFR and MVR with $N < 4$, even though $P_r(A^T)$ is smaller than that of NFP for each value of N, $P_r(T_{AB})$ grows faster than that of NFP. Therefore, we can see better performance for MFR and MVR in the one-hop throughput when $N < 5$.

In Fig. 13, we plotted the results of the normalized average progress $Z\sqrt{\lambda}$ for the slotted CSMA/CA-like protocol. It is observed that, as N grows, $Z\sqrt{\lambda}$ increases dramatically for MVR and MFR, but it increases and becomes stable for NFP.

The average delay D versus connectivity N using different strategies for the slotted CSMA/CA-like protocol is exhibited

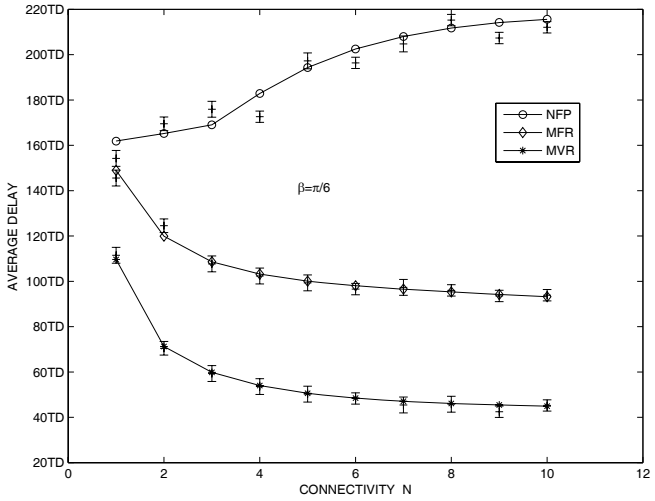

Fig. 14. Average delay D versus connectivity N for CSMA/CA-like protocol.

in Fig. 14. We can observe that D increases as N grows for NFP. NFP has the worst performance in average delay, since a node selects the nearest neighbour on its forward semicircle. It takes more hops than MFR and MVR to relay a packet to the destination. For MFR and MVR, a node selects the farthest neighbour on its forward semicircle. Therefore, as the network connectivity becomes higher, the average delay D decreases. MVR has the best performance in average delay, since it utilizes the power control to limit the interference range in each transmission, while maximizing the effective transmission distance by selecting a relay node with the maximum forward progress.

In general, the slotted CSMA/CA-like protocol has better network performance over the slotted ALOHA protocol in terms of the one-hop throughput and average forward progress. It sets aside the initiated portion of a time slot for the RTS/CTS exchange phase. If a node fails to receive a CTS packet successfully, it will refrain from transmitting data and save the network capacity for other nodes in the network. Indeed, the value of $P_r(A^T)$ is contingent upon the network performance during m-slot1 and m-slot2. Each node transmits data with a smaller $P_r(A^T)$ when the network is more congested during the RTS/CTS exchange phase and vice versa. By applying the slotted CSMA/CA-like protocol, the network becomes more resilient. However, this also requires more packet transmissions and power consumption. This can be a concern when nodes are battery-powered.

The results shown in Figs. 8-10, 12-14 correspond to $\beta = \frac{\pi}{6}$. Similar trends are observed when we use other values of β, but those results are omitted due to space limitations.

V. Conclusions

We have proposed a model to analyze the one-hop throughput and forward progress in wireless ad hoc networks with smart antennas. Our model can accommodate different values of the transmission range and interference range. It uses two parameters, namely a_R and a_β, to define the interference ratio. a_R is the ratio of the interference radius to the transmission radius, whereas a_β is the ratio of the interference angle to the transmission angle. Our results show that performance can be greatly improved by using smart antennas in place of omni-directional antennas. Adjustable transmission radius can also mitigate the interference in the network and ensure stability.

We have analyzed two MAC protocols, namely, slotted ALOHA and the slotted CSMA/CA-like protocol. For slotted ALOHA, NFP always yields the best one-hop throughput due to the use of the smallest possible transmission radius which induces the least interference. Meanwhile, it yields the least normalized average forward progress compared with the other two strategies, requiring more relays to deliver a message from a source to a destination. Since all nodes in the network share the same channel, more conflicts will occur due to more relays. However, NFP uses the least transmission radius for each transmission which counterbalances some of the network interference. On the contrary, MVR yields the best normalized average forward progress but the worse one-hop throughput compared with NFP. This implies fewer relays from a source to a destination, but a larger interference radius for each transmission.

With respect to the average delay from a source to a destination, MVR yields the best performance since it embraces a good tradeoff between the number of the relays and interference ranges. For the slotted CSMA/CA-like protocol, the network becomes more resilient by adapting the probability for data transmission. It has better network performance over the slotted ALOHA protocol in terms of the one-hop throughput and average forward progress. However, it also requires more packet transmissions and power consumption. This can be a concern when nodes are battery-powered.

References

[1] Y. J. Chang, Y. H. Ho, K. S. Dan, and U. H. Gang, "Enhanced Markov chain model and throughput analysis of the slotted CSMA/CA for IEEE 802.15.4 under unsaturated traffic conditions," *IEEE Trans. Veh. Technol.*, vol. 58, no. 1, pp. 473-478, Jan. 2009.

[2] R. R. Choudhury and N. H. Vaidya, "Deafness: a MAC problem in ad hoc networks when using directional antennas," in *Proc. IEEE ICNP 2004*, pp. 283-292, July 2004.

[3] R. Compton, *Adaptive Antennas: Concepts and Performance*. Prentice Hall, 1988.

[4] J. Deng, Y. S. Han, P. N. Chen, and P. K. Varshney, "Optimal transmission range for wireless ad hoc networks based on energy efficiency," *IEEE Trans. Commun.*, vol. 55, no. 9, pp. 1772-1782, Sep. 2007.

[5] J. H. He, Z. Y. Tang, H. H. Chen, and Q. Zhang, "An accurate and scalable analytical model for IEEE 802.15.4 slotted CSMA/CA networks," *IEEE Trans. Wireless Commun.*, vol. 8, no. 1, pp. 440-448, Jan. 2009.

[6] T. C. Hou and V. O. K. Li, "Transmission range control in multihop packet radio networks," *IEEE Trans. Commun.*, vol. COM-34, no.1, pp. 38-44, Jan. 1986.

[7] F. Huang, V. O. K. Li, and K.-C. Leung, "Adjustable transmission power in wireless ad hoc networks with smart antennas," in *Proc. IEEE GLOBECOM 2008*, Dec. 2008.

[8] E.-S. Jung and N. H. Vaidya, "A power control MAC protocol for ad hoc networks," *Wireless Netw.*, vol. 11, no. 1-2, pp. 55-66, Jan. 2005.

[9] R. Jurdak, C. V. Lopes, and P. Baldi, "A survey, classification and comparative analysis of medium access control protocols for ad hoc networks," *IEEE Commun. Surveys Tutorials*, vol. 6, no. 1, pp. 2-16, First Quarter 2004.

[10] E. D. Kaplan, ed., *Understanding GPS: Principles and Applications*. Boston, MA: Artech House, 1996.

[11] T. S. Kim and S. L. Kim, "Random power control in wireless ad hoc networks," *IEEE Commun. Lett.*, vol. 9, no. 12, pp. 1046-1048, Dec. 2005.

[12] C. B. Li and J. J. Garcia-Luna-Aceves, "Transmission scheduling in ad hoc networks with directional antennas," in *Proc. ACM MOBICOM 2002*, pp. 48-58, Sep. 2002.
[13] J. Li, C. Blake, D. Couto, H. Lee, and R. Morris, "Capacity of ad hoc wireless networks," in *Proc. ACM MOBICOM 2001*, pp. 61-69, July 2001.
[14] J. Liu, L. Li, and H. Z. Wang, "Investigation of different types of array structures for smart antennas," in *Proc. IEEE ICMMT 2008*, pp. 234-238, Dec. 2008.
[15] Q. Liu and J. Li, "Packet delivery through difficult wireless channel," in *Proc. IEEE MILCOM 2002*, vol. 1, pp. 530-535, Oct. 2002.
[16] H.-J. Perz and B. Walke, "Adjustable transmission power for mobile communications with ominidirectional and directional antennas in an one-and-multi-hop environment," in *Proc. IEEE Veh. Technol. Conf. 1991*, pp. 630-635, May 1991.
[17] K. S. Pour and A. Ephremides, "Stochastic approximation and directive antennas in wireless networks," in *Proc. IEEE Conf. Decision Control 1998*, pp. 1102-1105, Dec. 1998.
[18] R. Radhakrishnan, D. Lai, J. Caffery, and D. P. Agrawal, "Performance comparison of smart antenna techniques for spatial multiplexing in wireless ad hoc networks," in *Proc. 5th International Symp. Wireless Personal Multimedia Commun.*, vol. 1, pp. 168-171, Oct. 2002.
[19] S. M. Rokonuzzaman, R. Pose, and I. Gondal, "A framework for a QoS based adaptive topology control system for wireless ad hoc networks with multibeam smart antennas," in *Proc. International Symp. Parallel Distributed Process. Appl. 2008*, pp. 940-945, Dec. 2008.
[20] J. F. Shan, C. Zheng, H. Wang, and N. H. Yu, "An effective MAC scheme based on large interference range in mobile ad hoc networks," in *Proc. 6th International Conf. Machine Learning Cybernetics*, vol. 4, pp. 2145-2149, Aug. 2007.
[21] Y. Takatsuka, K. Nagashima, M. Takata, M. Bandai, and T. Watanabe, "A directional MAC protocol for practical smart antenna," in *Proc. IEEE GLOBECOM 2006*, Nov.-Dec. 2006.
[22] M. Watanabe, H. Mitsuhashi, M. Bandai, S. Obana, and T. Watanabe, "Empirical discussion on directional MAC protocols for ad hoc networks using practice smart antennas," in *Proc. IEEE ICC 2007*, pp. 3642-3647, June 2007.
[23] S. L. Wu, Y. C. Tseng, and J. P. Sheu, "Intelligent medium access for mobile ad hoc networks with busy tones and power control," *IEEE Trans. Commun.*, vol. 18, no. 9, pp. 1647-1657, Sep. 2000.
[24] J. Zander, "Slotted ALOHA multihop packet radio networks with directional antennas," *Electron. Lett.*, vol. 26, no. 25, pp. 2098-2100, Dec. 1990.
[25] S. A. Zekavat and C. R. Nasssar, "Smart antenna arrays with oscillating beam patterns: characterization of transmit diversity in semi-elliptic coverage," *IEEE Trans. Commun.*, vol. 50, no. 10, pp. 1549-1556, Oct. 2002.

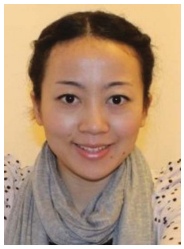

Fei Huang (S'07) was born in China in 1983. She received the B.Eng. degree in Electronic Engineering from University of Electronic Science and Technology of China, China, in 2005. She is currently a PhD student in the Department of Electrical and Electronic Engineering, The University of Hong Kong. Her research interests include smart antennas, performance analysis, and MAC protocol design in wireless ad hoc networks.

Ka-Cheong Leung (S'95–M'01) received the B.Eng. degree in Computer Science from the Hong Kong University of Science and Technology, Hong Kong, in 1994, the M.Sc. degree in Electrical Engineering (Computer Networks) and the Ph.D. degree in Computer Engineering from the University of Southern California, Los Angeles, California, USA, in 1997 and 2000, respectively. He worked as Senior Research Engineer at Nokia Research Center, Nokia Inc., Irving, Texas, USA from 2001 to 2002. He was Assistant Professor at the Department of Computer Science at Texas Tech University, Lubbock, Texas, USA, between 2002 and 2005. Since June 2005 he has been with the University of Hong Kong, Hong Kong, where he is currently Research Assistant Professor at the Department of Electrical and Electronic Engineering. His research interests include transport layer protocol design, wireless packet scheduling, routing, congestion control and quality of service guarantees in high-speed communication networks, content distribution, high-performance computing, and parallel applications.

Victor O. K. Li (S'80–M'81–SM'86–F'92) received SB, SM, EE and ScD degrees in Electrical Engineering and Computer Science from MIT in 1977, 1979, 1980, and 1981, respectively. He is Associate Dean of Engineering and Chair Professor of Information Engineering at the University of Hong Kong (HKU), and Guest Chair Professor of Wireless Communication and Networking at Tsinghua University, Beijing, China. He also served as Managing Director of Versitech Ltd., the technology transfer and commercial arm of HKU, and on the boards of Sunevision Holdings Ltd. and China.com Ltd. Previously, he was Professor of Electrical Engineering at the University of Southern California (USC), Los Angeles, California, USA, and Director of the USC Communication Sciences Institute. Sought by government, industry, and academic organizations, he has lectured and consulted extensively around the world. He has received numerous awards, including the PRC Ministry of Education Changjiang Chair Professorship at Tsinghua University, the UK Royal Academy of Engineering Senior Visiting Fellowship in Communications, the Croucher Foundation Senior Research Fellowship, and the Order of the Bronze Bauhinia Star, Government of the Hong Kong Special Administrative Region, China. He is a Registered Professional Engineer and a Fellow of the IAE, and the HKIE.